Structure Studies of Dimeric $[Pt_2(CN)_{10}]^{4-}$ Pentacyanoplatinum(III) and Monomeric Pentacyanoplatinum(IV) Complexes by EXAFS, Vibrational Spectroscopy, and X-ray Crystallography†

Farideh Jalilehvand,[‡] Mikhail Maliarik,[§,||] János Mink,*[,⊥,#] Magnus Sandström,*[,★] Andrey Ilyukhin,[||] and Julius Glaser[§]

Department of Chemistry, Stanford University, Stanford, California 94305-5080, Department of Chemistry, Inorganic Chemistry, The Royal Institute of Technology (KTH), S-100 44 Stockholm, Sweden, Kurnakov Institute of General and Inorganic Chemistry, Russian Academy of Sciences, Leninsky Prospect 31, Moscow 117907, Russia, Department of Analytical Chemistry, University of Veszprém, P.O. Box 158, H-8201, Veszprém, Hungary, Institute of Isotope and Surface Chemistry of the Hungarian Academy of Sciences, P.O. Box 77, H-1525 Budapest, Hungary, and Department of Structural Chemistry, Arrhenius Laboratory, University of Stockholm, SE−106 91 Stockholm, Sweden

Received: July 16, 2001; In Final Form: December 6, 2001

The structures of the dimeric bispentacyanoplatinate(III)*(*Pt−Pt*)* complex $[Pt_2(CN)_{10}]^{4-}$ and the pentacyanoplatinum(IV) species $[Pt(CN)_5(OH)]^{2-}$, $[Pt(CN)_5(H_2O)]^{-}$, and $[Pt(CN)_5I]^{2-}$ have been studied in aqueous solution by the EXAFS technique. A nonsupported Pt−Pt bond, 2.73(1) Å, connects two $Pt(CN)_5$ entities in the dimer. Normal coordinate analyses have been made on the basis of the Raman spectra, and the force constants have been used for discussions of the bonding. The metal−metal stretching force constants for the $[Pt_2(CN)_{10}]^{4-}$ complex, the $[(NC)_5Pt-Tl(CN)_n]^{n-}$ (n = 1, 2, and 3) complexes, and some other dimetallic complexes have been correlated with the metal−metal bond distances. In the $[Pt(CN)_5X]^{n-}$ complexes, the mean Pt−C bond distance of the pentacyanoplatinum group was found to increase, and the corresponding Pt−C force constants were found to decrease, with increasing donor ability of the ligand X in the order X = H_2O, OH, I, and $Pt(CN)_5$. The crystal structures of the compounds $Tl_2[Pt(CN)_5(OH)]$ and $K_2[Pt(CN)_5I]\cdot 0.6H_2O$ were determined by single-crystal X-ray diffraction techniques and used for comparisons with the EXAFS models. The Pt−I bond distance of the $[Pt(CN)_5I]^{2-}$ complex is 2.676(2) Å in the crystal structure and 2.66(1) Å in solution by EXAFS. A method is described for estimating the force constant for the metal−metal bond stretch in dimetallic complexes with heavy metal atoms, based on the use of an effective "spectroscopic" mass of the metal atoms in a diatomic model. The 18-electron rule is found to be useful for rationalizing the structures of the metal−metal bonded cyano complexes and a guideline in searching for metal cyano complexes analogous to those currently described.

Introduction

Metal−metal bonded complexes have received much attention because of their unusual properties and, in many cases, the difficulty to find simplifying models to predict and describe the bonding.[1] Extensively studied are the partially oxidized columnar stacks of square-planar $Pt(CN)_4^{2-}$ complexes with Pt−Pt distances of 2.8 to 3.0 Å,[2] as in the cation deficient $K_{1.75}Pt(CN)_4\cdot 1.5H_2O$ compound.[3] The metallic conductance and the structure of these linear chains reveal that the Pt atoms are chemically equivalent and, thus, in a single resonance partial oxidation state.[4] In other compounds, however, unequal Pt−Pt distances occur in the chains. These can possibly be described as mixed valence Pt^{II}-Pt^{III} compounds.[1] A number of singly metal−metal bonded diplatinum(III) complexes are now known, even though ligand bridges are also present in most cases.[1] Very few complexes with unsupported $Pt^{III}-Pt^{III}$ bonds have been reported.[5−8]

We have recently prepared and studied dimetallic $[(NC)_5Pt-Tl(CN)_n]^{n-}$ (n = 0, 1, 2, and 3) complexes with an unsupported metal−metal bond in aqueous solution.[9−12] Short Pt−Tl bond distances were found, 2.60(1), 2.62(1), and 2.64(1) Å, for n = 1, 2, and 3, respectively, and the ^{195}Pt and ^{205}Tl NMR chemical shifts revealed a gradual metal−metal electron transfer.[12] The results support a description with partial oxidation states of the metal atoms relative to the parent mononuclear complexes, and the species can be described as metastable intermediates in a two-electron-transfer reaction from platinum(II) to thallium(III). Vibrational spectra were interpreted by normal coordinate analyses and used for discussion of the delocalized bonding in these species,[12] which also have been the subject of theoretical studies.[13,14]

In our studies of oligonuclear platinum−thallium cyano complexes, we found the pentacyanoplatinum $Pt(CN)_5$ group to be a stable entity, appearing in the decomposition products from redox reactions involving the metal−metal bond.[15] Mostly, $[Pt^{IV}(CN)_5X]^{n-}$ complexes form with X = H_2O, OH^-, and CN^-,

† Part of the special issue "Mitsuo Tasumi Festschrift".
* To whom correspondence should be addressed.
‡ Stanford University.
§ The Royal Institute of Technology (KTH).
|| Russian Academy of Sciences.
⊥ University of Veszprém.
Institute of Isotope and Surface Chemistry of the Hungarian Academy of Sciences.
★ University of Stockholm.

10.1021/jp012712x CCC: $22.00
Published on Web 03/08/2002

as expected from the 18-electron rule, which often is used for coordination guidelines in organometallic chemistry.[16] An isolated $[Pt^{II}(CN)_5]^{3-}$ unit, consistent with the 18-electron rule, would require five-coordination. However, by connecting two $-Pt(CN)_5$ units with a single two-electron Pt−Pt bond in a $[Pt_2(CN)_{10}]^{4-}$ complex, the 18-electron rule is satisfied in six-coordination and the intermediate oxidation state Pt(III) stabilized. We previously reported the formation and NMR characterization of a dinuclear $[Pt_2(CN)_{10}]^{4-}$ species in aqueous solution.[15] Its structure is of special interest for our studies of redox reactions involving metal−metal bonds and interactions in cyano complexes.[12] This complex was recently characterized spectroscopically as a solid film of $Cu_2[Pt_2(CN)_{10}]$ prepared electrochemically.[17] Because we have not so far been able to obtain a crystalline compound of this species, EXAFS studies were performed on a dilute aqueous solution, and the result is reported in the present work.

In addition, EXAFS measurements and X-ray crystal structure determinations were performed for some pentacyanoplatinum species to further investigate the correlation between the structure, spectra, bond strength, and oxidation state in these systems. Results from solutions of $[Pt(CN)_5(OH)]^{2-}$, $[Pt(CN)_5(H_2O)]^{-}$, and $[Pt(CN)_5I]^{2-}$ complexes and of the solid compounds $Tl_2[Pt(CN)_5(OH)]$ and $K_2[Pt(CN)_5I]\cdot 0.6H_2O$, all containing tetravalent $[Pt(CN)_5X]^{n-}$ complexes, are reported. We have found no previous reports on crystal structures of $[Pt(CN)_5X]^{n-}$ complexes.

Previously, vibrational spectra of pentacyanohaloplatinum(IV) complexes, $[Pt(CN)_5X]^{2-}$ (X = Cl, Br, I, and CN) in the solid state and in solution showed some halide dependence of the Pt−C stretching frequencies.[18] It was concluded that the *trans*-influence (weakening of the axial Pt−C bond trans to the ligand X) decreases in the order I > Br > Cl > CN. In our previous spectroscopic characterization of the pentacyanohaloplatinum complexes, the NMR spectra showed different chemical shifts and spin−spin coupling constants for the axial and equatorial cyano ligands.[10,15] A pronounced trans influence was found for the $^{195}Pt-{}^{13}C_{axial}$ spin−spin coupling constant, $^1J_{Pt-C}$, which decreases in the order $H_2O > Cl^- > Br^- > I^- > OH^- > CN^-$. In the present work, normal coordinate calculations have been made to obtain a more detailed picture of the bonding in these species.

Experimental Section

Preparations. Aqueous solutions of the complexes $[Pt(CN)_5(OH)]^{2-}$ and $[Pt(CN)_5(H_2O)]^{-}$ were obtained as described previously from redox decomposition of the solid $TlPt(CN)_5$ compound.[15,19] The $[Pt_2(CN)_{10}]^{4-}$ complex can be prepared in aqueous solution either from a redox reaction occurring between the $[Tl^{III}(CN)_n]^{3-n}$ and $[Pt(CN)_4]^{2-}$ (in excess) complexes[15] or by photoredox decomposition of a trinuclear $[(NC)_5Pt-Tl-Pt(CN)_5]^{3-}$ complex in aqueous solution.[20] The $[Pt(CN)_5I]^{2-}$ complex was prepared according to a procedure described in the literature.[15] The concentration for the EXAFS studies was 0.10 mol dm^{-3} of $[Pt(CN)_5(OH)]^{2-}$, $[Pt(CN)_5(H_2O)]^{-}$, and $[Pt(CN)_5I]^{2-}$ and 0.035 mol dm^{-3} of $[Pt_2(CN)_{10}]^{4-}$. The solid compounds were prepared as follows.

$Tl_2[Pt(CN)_5(OH)]$. Colorless crystals were formed when slowly evaporating a $[Pt(CN)_5OH]^{2-}$ solution containing Tl^+ ions.[20]

$K_2[Pt(CN)_5I]\cdot 0.6H_2O$. Pale yellow crystals were obtained upon slow evaporation of an aqueous solution of the $[Pt(CN)_5I]^{2-}$ complex.

The platinum content of the solutions and the solid compounds was determined by means of ICP (inductively coupled plasma) spectrophotometry, and carbon and nitrogen (in the solid) contents were determined by elemental analyses (Mikro-Kemi AB, Uppsala, Sweden).

TABLE 1: Crystallographic Data

compound	$Tl_2[Pt(CN)_5OH]$	$K_2[Pt(CN)_5I]\cdot 0.6H_2O$
formula weight	750.94	541.1
wavelength (Å)	0.71073 (Mo Kα)	
crystal system	monoclinic	
space group	$P2_1/n$ (No. 14)	
unit cell dimensions		
a (Å)	6.636(1)	7.688(2)
b (Å)	20.442(4)	13.259(3)
c (Å)	8.534(2)	12.810(3)
β (deg)	107.45(3)	91.83(3)
volume ($Å^3$)	1104.4(4)	1305.1(5)
Z, calculated density (g/cm^3)	4, 4.510	4, 2.754
μ (cm^{-1})	41.72	13.73
F(000)	1256	960
reflections collected/unique	2806/1960	2343/1404
refinement method	full-matrix least-squares on F^2	
no. of parameters	127	136
goodness-of-fit on F^2	1.075	1.046
R_1, wR2 [all data][a]	0.034, 0.075	0.049, 0.116

[a] Reliability indices $R = \sum||F_o| - |F_c||/\sum|F_o|$; $wR = [\sum w(|F_o| - |F_c|)^2/\sum(w|F_o|)^2]^{1/2}$.

TABLE 2: Bond Distances in the Crystal Structures of $Tl_2[Pt(CN)_5(OH)]$ and $K_2[Pt(CN)_5I]\cdot 0.6H_2O$[a]

$[Pt(CN)_5(OH)]^{2-}$	distance/Å	$[Pt(CN)_5I]^{2-}$	distance/Å
Pt−C1	1.968 (13)	Pt−C1	1.990 (16)
Pt−C2	1.996 (12)	Pt−C2	1.989 (15)
Pt−C3	2.023 (11)	Pt−C3	2.056 (17)
Pt−C4	2.011 (11)	Pt−C4	1.992 (18)
Pt−C5	2.029 (14)	Pt−C5	1.974 (17)
Pt−O	2.027 (7)	Pt−I	2.676 (2)

[a] For notations, see Figure 1.

NMR and Raman Spectroscopy. ^{195}Pt and ^{13}C spectra were used to characterize the platinum complexes in solution. All NMR spectra were recorded with a Bruker AM400 spectrometer at a probe temperature of 298 (±0.5) K. Typical NMR parameters for the spectra can be found in our recent publications.[9,10,15] Raman spectra were excited using the 514.5 nm green line from a Coherent Radiation Laboratories Innova 90-5 argon ion laser, as described previously.[10] For some NMR and Raman measurements, ^{13}CN-enriched (99%) solutions were used.

Force Constant Calculations. Wilson's GF matrix method was used for the calculation of force constants, with the use of a specially developed PC-based program package.[21] Bond distances were taken from Table 3 and regular octahedral geometry was assumed. The internal coordinates are defined in Figure 6. The initial force constants both for the dimeric Pt(III) and monomeric Pt(IV) complexes were adapted from our earlier analyses of the dimetallic $[(NC)_5Pt-Tl(CN)_n]^{n-}$ (n = 1, 2, and 3) complexes.[12]

Crystallography. A Syntex $P2_1$ single-crystal diffractometer was used for the data collection at ambient temperature. The SHELX97 program was used for solving and refining the crystal structures.[22] Further crystallographic data and details of the structure determination for the compounds $Tl_2[Pt(CN)_5(OH)]$ and $K_2[Pt(CN)_5I]\cdot 0.6H_2O$ are given in Table 1, and selected bond distances are given in Table 2.

EXAFS Data. Pt L_{III}-edge EXAFS data were collected in transmission mode at the Stanford Synchrotron Radiation Laboratory (SSRL) at the experimental station 4-1. The experimental conditions were similar to those described previously.[12,19,23] The energy calibration was made by simultaneously scanning a Pt foil for which the first inflection point was set to

SCHEME 1: EXAFS Backscattering Pathways in a Linear Pt−C−N Unit where There Are Two Equivalent Triple Scattering Pathways ($n_{leg} = 3$)

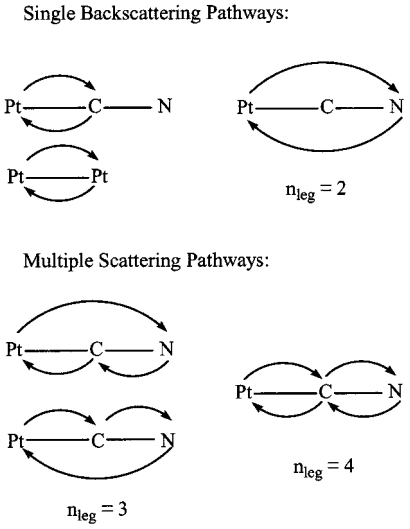

11 564 eV. In the samples containing thallium, the usable range for the Pt L_{III}-edge EXAFS measurements is limited to $k \approx 15$ Å^{-1} by the Tl L_{III}-edge at 12 658 eV. Typically, 3−4 scans were averaged for each sample. Solution cells with Mylar or thin (~40μm) glass windows and Vitone or Teflon spacers (3−5 mm) were used. The solid sample was diluted with boron nitride (BN) in order to obtain an edge step of approximately one logarithmic unit.

The EXAFS data were extracted using standard procedures for preedge subtraction, data normalization, and spline removal, by means of the WinXAS computer program.[24] The k^3-weighted EXAFS oscillations were Fourier transformed over the k range 2.6−14.1 Å^{-1}, using a Bessel window. This generally resulted in two major peaks corresponding to Pt−C and Pt−N distances. However, the second peak was found to be dominated by strong multiple scattering from several pathways. Linear configurations of ligand atoms, as for the cyano ligands, are known to enhance the multiple scattering by forward scattering of the intervening atom.[25] To be able to extract reliable structural parameters from the complexes in the current study, we developed and carefully tested models by means of the ab initio FEFF code,[25] describing the strong multiple scattering as a sum of contributions from separate selected backscattering pathways with a minimum of parameters.[12,19]

The model found to satisfactorily account for the experimental data from coordinated cyano ligands consists of the single backscattering from Pt−C to the first peak and, in the second peak, a dominating triple Pt−C−N ($n_{leg} = 3$) interaction, a quadruple Pt−C−N ($n_{leg} = 4$) contribution, and a minor contribution from the single Pt−N backscattering (Scheme 1). For all of the three paths involving the nitrogen atom, a mean Pt−N distance and a common Debye−Waller factor could be used in a least-squares refinement procedure. Theoretical phase and amplitude functions for the single and multiple scattering pathways described in the model were calculated by means of the FEFF7 program.[25] After Fourier filtering and back-transforming the real space range including the Pt−C and Pt−N peaks (from 1.1 to 8.0 Å), the resulting k^3-weighted EXAFS function, $k^3\chi(k)$, was used for least-squares refinements of interatomic model parameters, Table 3.

The amplitude of the EXAFS model function is directly proportional to both the frequency of the distances and the amplitude reduction factor, S_0^2. Therefore, the known coordination numbers were used for the model compounds in order to obtain experimental S_0^2 values by least-squares refinements. The S_0^2 values obtained were between 1.2 and 1.3, somewhat higher than expected theoretically (about 0.8−0.9). We observed a similar effect before.[12,26] One reason can be fluorescence radiation from the sample adding to the signal in the monitor I_0 ion chamber and thereby increasing the amplitude of the oscillations.[26] Another reason is that for cyano complexes with backscattering parameters calculated in this way we have sometimes obtained S_0^2 values higher than 1, with a simultaneous increase in the Debye−Waller factor.[12]

The estimated standard deviations s for the refined parameters given in Table 3 are obtained from the noise level at high k of the zero-weighted EXAFS function and do not include systematic errors of the measurements. However, systematic variations in the refined parameters, including the shift in the E_0 value (for which $k = 0$), using different models and data ranges, indicate that the accuracy of the absolute values of the bond distances given for the separate complexes is within ±0.02 Å. The errors given for the bond distances in the text represents the total estimated accuracy for the EXAFS results.

Results

I. Structures in the Solid State. A. $K_2[Pt(CN)_5I]\cdot 0.6H_2O$. In the crystal structure, discrete $[Pt(CN)_5I]^{2-}$ complexes are formed with a well-determined Pt−I distance of 2.676(2) Å (Table 2). The Pt−C distances to the five cyano ligands are less precise with a mean value of 2.00 Å, and the thermal ellipsoids show the main displacements of the carbon and nitrogen atoms to be perpendicular to the bond directions (Figure 1). The large displacements of the nitrogen atoms may cause the C−N distances to appear too short,[27] and the average value is 1.13 Å instead of that expected, 1.15−1.16 Å.[28−30] A disordered water molecule with an occupancy factor estimated to 0.6 from the least squares refinements is also found in the structure. The two closest distances between the water oxygen atom and the surrounding potassium ions are 2.65 and 2.83 Å.

B. $Tl_2[Pt(CN)_5(OH)]$. The crystal structure shows that five carbon atoms of the cyano ligands and the oxygen atom of a hydroxo group form a slightly distorted octahedron around the platinum atom, giving rise to discrete $[Pt(CN)_5(OH)]^{2-}$ complexes. The Pt−O distance 2.027(7) Å (Table 2) is obtained for an elongated thermal ellipsoid of the oxygen atom perpendicular to the bond direction (Figure 1). The oxygen atom probably forms a weak hydrogen bond to the cyanide nitrogen of another $[Pt(CN)_5(OH)]^{2-}$ complex (O1···N4 3.02 Å).

The Pt−C distances are distributed within the range of 1.968(13)−2.029(14) Å (Table 2), with the shortest distance Pt−C1 to the cyano ligand trans to the oxygen atom. Although the positions of the nitrogen atoms all are represented by large thermal ellipsoids, the mean C−N distance is 1.15 Å (range 1.13−1.17 Å). The Pt−C−N bond angles appear in the range of 169−176° corresponding to a mean Pt−N distance of 3.15 Å.

The EXAFS data for the $[Pt(CN)_5(OH)]^{2-}$ complex in the solid state give a mean Pt−C bond distance of 1.99(1) Å and a Debye−Waller factor corresponding to a root-mean-square displacement of $\sigma = 0.06(1)$ Å in the distance (Table 3). Thus, the trans influence indicated by the crystal structure data is too small to be discerned by EXAFS. The Pt−O bond distance could not be resolved from the Pt−C distances and was in the least-squares refinements held constant at the crystal structure value, 2.027 Å. The EXAFS refinement gives a mean Pt−N distance, 3.15(1) Å, in agreement with the crystal structure value, but a

TABLE 3: Pt L_{III}-Edge EXAFS[a]

sample	scattering pathway[b]	multiplicity	distance *r*/ Å	D−W σ^2/Å^2	ΔE_o/eV	residual[d]
$[Pt(CN)_5(OH)]^{2-}$	Pt−C	5	1.996 (4)	0.0034 (1)	7.4 (3)	17.0
0.1 M	Pt−O	1	2.028[b]	0.0017 (1)		
	Pt−N	5	3.152	0.0043		
	Pt−C−N (3)	10	3.152 (1)	0.0043 (1)		
	Pt−C−N (4)	5	3.152	0.0043		
$Tl_2[Pt(CN)_5OH]$	Pt−C	5	1.986 (4)	0.0036 (2)	7.5 (4)	14.2
solid	Pt−O	1	2.027[c]	0.0009 (6)		
	Pt−N	5	3.146	0.0049		
	Pt−C−N (3)	10	3.146 (2)	0.0049 (2)		
	Pt−C−N (4)	5	3.146	0.0049		
$[Pt(CN)_5(H_2O)]^-$	Pt−C	5	1.986 (2)	0.0040 (2)	7.2 (4)	16.0
0.1 M	Pt−O	1	2.037[c]	0.0025[b]		
	Pt−N	5	3.144	0.0048		
	Pt−C−N (3)	10	3.144 (2)	0.0048 (2)		
	Pt−C−N (4)	5	3.144	0.0048		
$[Pt(CN)_5I]^{2-}$	Pt−C	5	2.002 (2)	0.0029 (2)	7.1 (4)	14.2
0.1 M	Pt−I	1	2.664 (2)	0.0039 (2)		
	Pt−N	5	3.154	0.0043		
	Pt−C−N (3)	10	3.154 (2)	0.0043 (2)		
	Pt−C−N (4)	5	3.154	0.0043		
$[Pt_2(CN)_{10}]^{4-}$	Pt−C	5	2.008 (2)	0.0033 (1)	7.1 (3)	16.0
0.035 M	Pt−Pt	1	2.729 (3)	0.0045 (3)		
	Pt−N	5	3.160	0.0044		
	Pt−C−N (3)	10	3.160 (2)	0.0044 (2)		
	Pt−C−N (4)	5	3.160	0.0044		

[a] Results of model fitting to k^3-weighted and Fourier-filtered data (range r = 1.1 to 8.0 Å), with standard deviations estimated from noise at high k in zero-weighted unfiltered data. [b] Distances and Debye−Waller σ^2-parameter for all pathways of the "Pt−N" peak are coupled to the Pt−C−N 3-legged pathway (cf. Scheme 1). [c] Fixed value from crystal structures. [d] For definition, see ref 24.

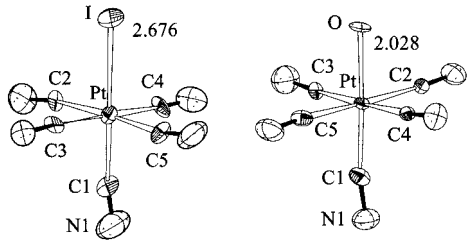

Figure 1. $[Pt(CN)_5I]^{2-}$ and $[Pt(CN)_5(OH)]^{2-}$ complexes in the crystal structures of $K_2[Pt(CN)_5I]\cdot 0.6H_2O$ and $Tl_2[Pt(CN)_5(OH)]$. The Pt−I and Pt−O distances are given in Å.

somewhat shorter (0.015 Å) mean Pt−C distance. This could be a result from more dominant contributions from the most tightly bonded cyano ligands. Figure 2 shows the contributions from the separate scattering paths in the model for the $[Pt(CN)_5(OH)]^{2-}$ and the $[Pt(CN)_5I]^{2-}$ complexes.

II. Structure of the Complexes in Solution. A. EXAFS Analyses. The parameters for the fitted models for the three mononuclear complexes $[Pt(CN)_5X]^{n-}$, X = H_2O, OH^-, and I^-, and the binuclear complex $[Pt_2(CN)_{10}]^{4-}$ are given in Table 3. As previously, the axial and equatorial Pt−C distances could not be resolved, and a mean Pt−C value, 2.01(1) Å, was obtained with similar Debye−Waller factors as for other platinum−cyano complexes.[12] The mean Pt−N distance is in all cases 1.15−1.16 Å longer than that of Pt−C, consistent with an almost linear coordination.[28−30] Also, the Pt−O and Pt−C distances are too close to be refined independently. Therefore, for the solution complex $[Pt(CN)_5(OH)]^{2-}$, the Pt−O distance 2.027 Å, obtained from the crystal structure of $Tl_2[Pt(CN)_5(OH)]$, was used. For the aqua complex $[Pt(CN)_5(H_2O)]^-$ the Pt−O distance was assumed to be slightly longer, 2.037 Å (Table 3). The correlation between the Pt−C and Pt−O distances is not strong, and a variation of ±0.02 Å in the Pt−O distance gave a shift of the mean Pt−C distance less than 0.01 Å. For the $[Pt(CN)_5I]^{2-}$ complex, the Pt−I contribution has its highest amplitude at high k values which facilitates the evaluation (cf. Figure 2b). The Pt−I bond distance obtained, 2.66(1) Å (Table 3), is close to the crystal structure value, 2.676(2) Å (Table 2).

Figure 3 shows the EXAFS spectrum of the $[Pt_2(CN)_{10}]^{4-}$ complex in 0.035 M aqueous solution, with separate contributions for the different backscattering paths for the structure proposed in Figure 4. The increasing amplitude at high k values of the Pt−Pt contributions to the EXAFS oscillations allowed a determination of the metal−metal bond distance to 2.73(1) Å.

B. Vibrational Spectra. 1. The $[Pt_2(CN)_{10}]^{4-}$ Complex. Assignment of Vibrational Frequencies. The frequencies obtained from Raman measurements of the $[Pt_2(^{12}CN)_{10}]^{4-}$ and $[Pt_2(^{13}CN)_{10}]^{4-}$ complexes in aqueous solution are given in Table 4. The Raman spectra are presented in Figure 5. Comparison with previous results from a vibrational study of pentacyanohalo complexes, including the $[Pt(CN)_5I]^{2-}$ complex[18] and our normal coordinate analyses of the dimetallic $[(NC)_5Pt-Tl(CN)_n]^{n-}$ (n = 0−3) cyano complexes[12] allowed assignments of the reported frequencies. Results of normal coordinate calculations have also been used to support the results given in Tables 4 and 5.

1.1. C−N Stretchings. A regular $[Pt_2(CN)_{10}]^{4-}$ complex belongs to point groups D_{4d} (staggered) or D_{4h} (eclipsed), depending on its conformation. The vibrational selection rules are identical for both point groups, and for simplicity, the D_{4h} symmetry was used for further analyses. A point group analysis shows 44 fundamental modes belonging to the following symmetry species: 7 A_{1g} + 1 A_{2g} + 4 B_{2g} + 8 E_g + A_{1u} + 7 A_{2u} + 2 B_{1u} + 4 B_{2u} +8 E_u.

For the CN stretching vibrations, four Raman active bands (2 A_{1g} + B_{1g} + E_g) are expected, of which the two A_{1g} modes are polarized. Curve fitting revealed six Raman bands in the C−N stretching region for the solution spectra of the $[Pt_2(^{12}CN)_{10}]^{4-}$ complex and seven bands for $[Pt_2(^{13}CN)_{10}]^{4-}$ (Figure 5). For the natural abundance $[Pt_2(^{12}CN)_{10}]^{4-}$ complex, careful analysis revealed that the polarized band at 2208 cm^{-1} belongs to an impurity of $[Pt(^{12}CN)_6]^{2-}$ and the shoulder at 2148 cm^{-1}

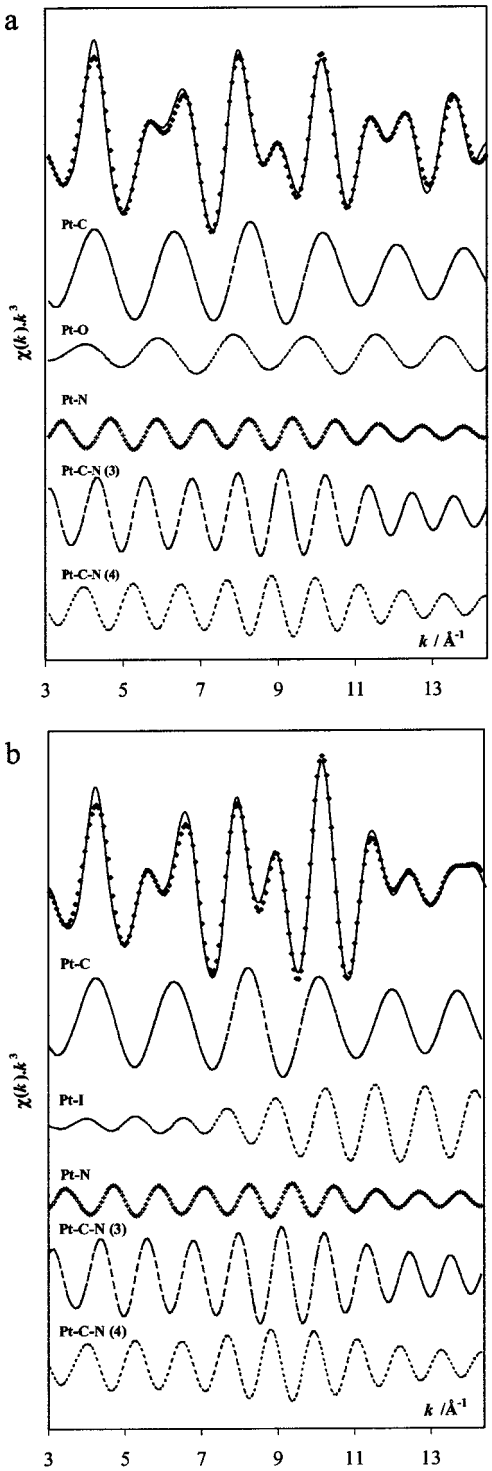

Figure 2. Pt L_{III}-edge EXAFS data, k^3-weighted and Fourier-filtered, for (a) the solid $Tl_2[Pt(CN)_5(OH)]$ compound (solid line) and (b) the $[Pt(CN)_5I]^{2-}$ complex in solution, showing the overall model fit (♦) and separate contributions (cf. Table 3).

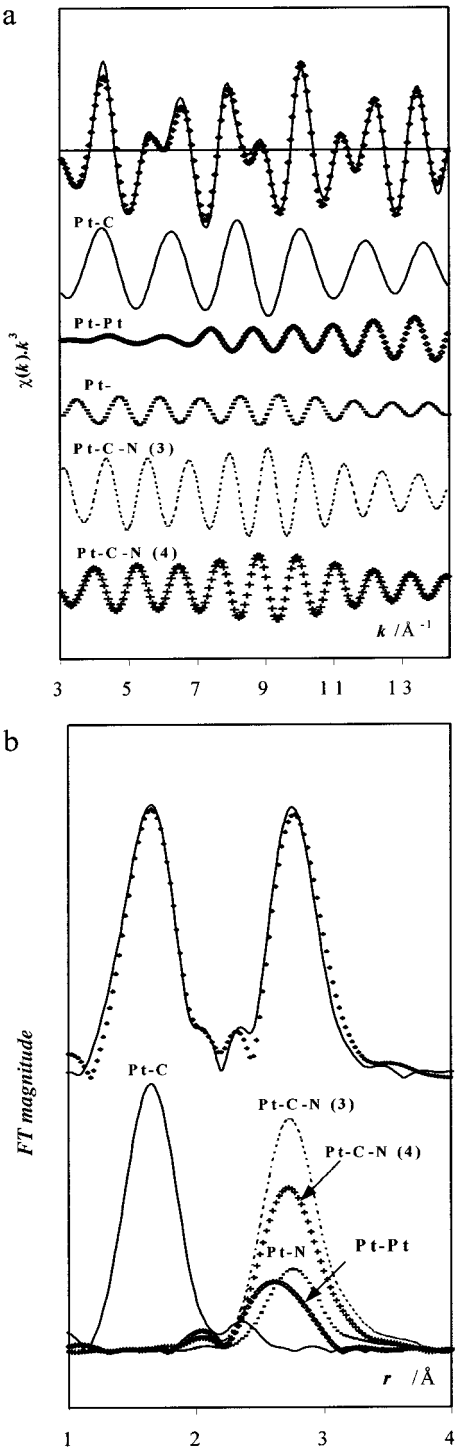

Figure 3. (a) Pt L_{III}-edge EXAFS k^3-weighted and Fourier-filtered data of the $[Pt_2(CN)_{10}]^{4-}$ complex in 0.035 M aqueous solution: top trace with model fit (♦) and contributions from separate scattering paths below (cf. Table 3). (b) Fourier transforms of the EXAFS functions in Figure 3a.

originates from some amount of $[Pt(^{12}CN)_4]^{2-}$. The strong band at 2161 cm^{-1} hides the totally symmetric C−N stretching mode of the $[Pt(^{12}CN)_4]^{2-}$complex around 2165 cm^{-1}. In a similar way, the two features observed in the Raman spectrum of $[Pt_2(^{13}CN)_{10}]^{4-}$ at 2158 and 2062 cm^{-1} are due to $[Pt(^{13}CN)_6]^{2-}$ and $[Pt(^{13}CN)_4]^{2-}$ impurities, respectively. The strongly polarized line at 2102 cm^{-1} is the A_{1g} mode of the $[Pt(^{13}CN)_4]^{2-}$ complex.

As a result, in this region, only three intensive Raman bands remained that could be assigned to the dimeric $[Pt_2(^{12}CN)_{10}]^{4-}$ complex. The two polarized bands at 2192 and 2161 cm^{-1} correspond to the equatorial and axial symmetric stretching (A_{1g}) modes, respectively. For the ^{13}CN-substituted complex, the polarized bands at 2143 and 2117 cm^{-1} can be assigned similarly. The third depolarized band in the $[Pt_2(^{12}CN)_{10}]^{4-}$ spectrum at 2177 cm^{-1} (2129 cm^{-1} for ^{13}C) should belong either to the E_g or B_{1g} equatorial CN stretching modes. In our previous paper, this band was reported as polarized;[15] however, after correction for the instrumental wavelength dependence of the observed polarizabilities, it clearly is depolarized. According

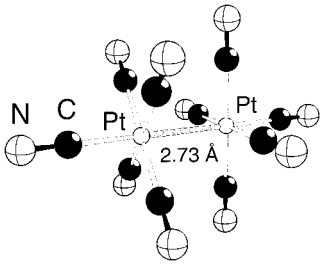

Figure 4. Proposed structure of the $[Pt_2(CN)_{10}]^{4-}$ complex in aqueous solution.

to our calculations, the separation of the E_g and B_{1g} equatorial CN stretching modes is about 11−13 cm^{-1} (cf. Table 5), comparable to the natural half width of the bands in this spectral region, which is about 10−12 cm^{-1}. A carefully made curve fitting showed weak bands at 2185 and 2134 cm^{-1} for the ^{12}CN and ^{13}CN complexes, respectively. Accordingly, these frequencies can be assigned as the B_{1g} mode. Very similar depolarized Raman bands were observed for $[Pt(CN)_5I]^{2-}$ at 2187.7 and 2179.5 cm^{-1} for the B_1 and E symmetry species of the CN stretching modes, respectively.

In aqueous solution, it is difficult to resolve such strongly overlapping vibrational features. To distinguish between minor bands from natural abundance isotopic species and those from impurities, a normal coordinate calculation was performed for one ^{13}CN cyano ligand substituted in an equatorial or axial position of the $[Pt_2(^{12}CN)_{10}]^{4-}$ complex. The corresponding calculation was made for ^{12}CN substitution in the fully ^{13}CN labeled complex. The results for the CN stretching modes are summarized in Table 6. The point group symmetry of $[Pt_2(CN)_{10}]^{4-}$ decreases to C_s or C_{4v} for equatorial or axial monosubstitution, respectively. The equatorial substitution leads to strong frequency shifts and splitting of the doubly degenerate E_g modes. For the $[Pt_2(^{12}CN)_{10}]^{4-}$ complex, the band at 2171 cm^{-1} moves to 2129 cm^{-1}, and for $[Pt_2(^{13}CN)_{10}]^{4-}$, the band moves from 2123 to 2181 cm^{-1}. Also the A_{2u} and B_{2u} normal modes showed weak isotopic effects.

According to these results, the weak feature listed in Table 4 at 2129 cm^{-1} can be attributed to the natural abundance of ^{13}CN cyano ligands in equatorial positions. Similarly, for the $[Pt_2(^{13}CN)_{10}]^{4-}$ complex, the ^{12}CN monosubstituted isotopomer showed a weak band at 2174 cm^{-1}.

For axial substitution, the isotopic effect is purely localized to the axial vibrations, and as a consequence, both the A_{1g} and A_{2u} species become IR and Raman active. Statistically, the axial CN stretching band intensity should be about 4 times weaker than for equatorial substitution. It was not possible to detect these bands which are expected from the calculations to occur at about 2113 and 2160.5 cm^{-1}.

1.2. Pt−C Stretchings. The Raman spectral features in the region containing Pt−C stretchings and Pt−C−N linear bendings are difficult to resolve when spectra are recorded in aqueous solution. It was found in our previous study of the dimetallic $[(NC)_5Pt-Tl(CN)_n]^{n-}$ ($n = 0-3$) species[12] that all Pt−C stretching modes for the $Pt(CN)_5$ units are observed within two broad bands around 460 and 415 cm^{-1}. Consequently, the two polarized bands in the $[Pt_2(^{12}CN)_{10}]^{4-}$ spectrum at 466 and 400 cm^{-1} can be assigned to symmetric Pt−C stretchings in the equatorial plane (A_{1g}) and to the axial Pt−C stretching (A_{1g}), respectively. The slightly shifted bands for ^{13}CN species at 461 and 395 cm^{-1} should correspond to the above two A_{1g} modes. In the solid $M_2[Pt(CN)_5X]$ complexes, the B_1 equatorial Pt−C stretching mode was obtained very close to or slightly higher than the A_1 mode.[18] Accordingly, a very weak shoulder at 471 cm^{-1} can be assigned as the B_{1g} mode for $[Pt_2(^{12}CN)_{10}]^{4-}$, but for $[Pt_2(^{13}CN)_{10}]^{2-}$, the strong A_{1g} band at 461 cm^{-1} prevented the observation of a similar feature.

The calculated E_g mode gives a band at 421.5 cm^{-1}, which is close to the observed 429 cm^{-1} band. Because the bands at 466 and 400 cm^{-1} are not very strongly polarized (depolarization ratio 0.53 and 0.43, respectively), it seems likely that they overlap with weak depolarized bands of asymmetric vibrations.

1.3. Pt−C−N Deformations. Our calculations show that several bands belonging to Pt−CN linear bending modes are expected in the 300−510 cm^{-1} region (cf. Table 5). The weak polarized band at 503 cm^{-1} is the best candidate for the A_{1g} mode (ν_5). The other two Raman active "out-of-plane" linear bendings at 429 (E_g) and 333 cm^{-1} (B_{1g}) were assigned based on the results of the calculations. The axial PtCN deformations were always observed close to 400 cm^{-1}.[12,19] The calculations gave a frequency at 397.5 cm^{-1}; therefore, the band at 400 cm^{-1} was assigned to this E_g mode (cf. Table 5). The "in-plane" equatorial PtCN deformation mode (E_g) was ascribed to the 477 cm^{-1} band. The band at 333 cm^{-1} can be assigned to both the B_{1g} and B_{2g} modes. The calculation resulted in the same frequency 332.1 cm^{-1} of these two modes (cf. Table 5).

1.4. Pt−Pt Stretching. This vibration gives one of the strongest polarized Raman bands at 145 cm^{-1}, which for $[Pt_2(^{13}CN)_{10}]^{2-}$ showed a slight isotopic shift to 144 cm^{-1}.

1.5. Skeletal Deformations. In the range expected for skeletal deformation modes (below 140 cm^{-1}), no low-frequency bands were observed. In addition to the 31 high-frequency fundamentals listed in Table 6, an additional 18 calculated frequencies were expected as CPtC or PtPtC deformations in the range from 126 to 43 cm^{-1}. Skeletal deformation modes involve $A_{1g} + B_{2g} + 3E_g + 2A_{2u} + B_{1u} + B_{2u} + 3E_u$ species. The torsional mode (A_{1u}) of the two pentacyano-platinum groups is omitted.

2. $[Pt(CN)_5(H_2O)]^-$ and $[Pt_2OH(CN)_5]^{2-}$. Assignment of Vibrational Frequencies. 2.1. C−N Stretchings. The Raman data for the complexes in aqueous solutions are included in Table 7. According to the C_{4v} local symmetry of the $Pt(CN)_5$ entity, four fundamentals ($2A_1 + B_1 + E$) are expected in the CN stretching region. The strongest polarized Raman band is obviously due to the symmetric stretching mode (ν_1) of the equatorial CN groups.

As a general rule for $Pt(CN)_5$ groups, the next highest depolarized Raman feature around 2190 cm^{-1} refers to the B_1 mode (ν_9).[12,18,19] It is rather difficult to obtain the exact position of the axial CN stretching band (ν_2), because of its overlap with the B_1 (ν_9) or E (ν_{15}) modes. Generally, these three bands, ν_2, ν_9, and ν_{15} have been observed in a very narrow (∼10 cm^{-1}) spectral range in the aqueous solution spectra of $[Pt(CN)_5X]^{2-}$ (X = Cl, Br, and I).[12,18] Therefore, the weak shoulders on the low-frequency side of the B_1 mode, at 2194 and 2176 cm^{-1}, have been assigned to A_1 axial CN stretching vibrations for the $[Pt(CN)_5(H_2O)]^-$ and $[Pt(CN)_5OH]^{2-}$ complexes, respectively (Table 7). The antisymmetric E mode (ν_{15}) is the most intense infrared band, which is the best argument for the assignment. Because we could not record IR spectra of the aqueous solutions, the same value was assumed for ν_{15} as for the axial CN stretching mode (ν_2). The remaining two weak features at 2167 and 2148 cm^{-1} belong to traces of the $[Pt(CN)_4]^{2-}$ complex of the starting material.

2.2. Pt−O Stretching Vibrations. These bands are generally broad and not very intense in a Raman spectrum, and polarization data were difficult to obtain for these A_1 modes. The Pt−OH stretching frequency of $[Pt(CN)_5(OH)]^{2-}$ is found as a distinct band at 546 cm^{-1}, whereas the Pt−OH_2 frequency in

TABLE 4: Raman Frequencies from Aqueous Solutions with $[Pt_2(CN)_{10}]^{4-}$ Complexes

$[Pt_2(^{12}CN)_{10}]^{4-}$			$[Pt_2(^{13}CN)_{10}]^{4-}$ (~99% enrichment)		
band position (cm^{-1})	rel intensity	depolarization ratio	band position (cm^{-1})	rel intensity	assignment[a]
2208	15	0.12	2158	44	$[Pt(CN)_6]^{2-}$ impurity
			2174	3	^{12}CN equatorial stretching (impurity)
2192	100	0.05	2143	100	CN symm. stretch equatorial
2185[b]	vvw		2134[b]	vvw	CN asymm. stretch equatorial
2177	33	0.76	2129	36	CN asymm. stretch equatorial
2161	52	0.41	2117	74	CN symm. stretch axial
2148	9		2101	29	$[Pt(CN)_4]^{2-}$ (impurity)
2129	1				^{13}CN equatorial stretching from 2177 cm^{-1} band (natural abundance)
628	12	0.75	628	50	ClO_4^- (ν_4, F_2)
518	vvw		508	vvw	
503	19	0.06	488	28	PtCN linear bending
477	vvw, sh		(461)		PtCN linear bending
471	vvw, sh		(461)		PtC stretch
466	26	0.53	461	100	PtCN linear bend, Pt−C equatorial stretch, ClO_4^- (ν_2, E)
446[b]	vvw		443[b]	vvw	PtC linear bend
429			430	20	PtCN linear bending
420	vvw, sh		411	vvw, sh	
400	25	0.43	395	29	PtCN linear bending, Pt−C axial stretching
333	2	0.36	318	3	PtCN linear bending
145	70	0.29	144	60	Pt−Pt stretching

[a] Tentative assignment in D_{4h} symmetry for $[Pt_2(CN)_{10}]^{4-}$. Abbreviations for intensity are w, weak; v, very; and sh, shoulder. [b] Frequencies obtained by curve fitting.

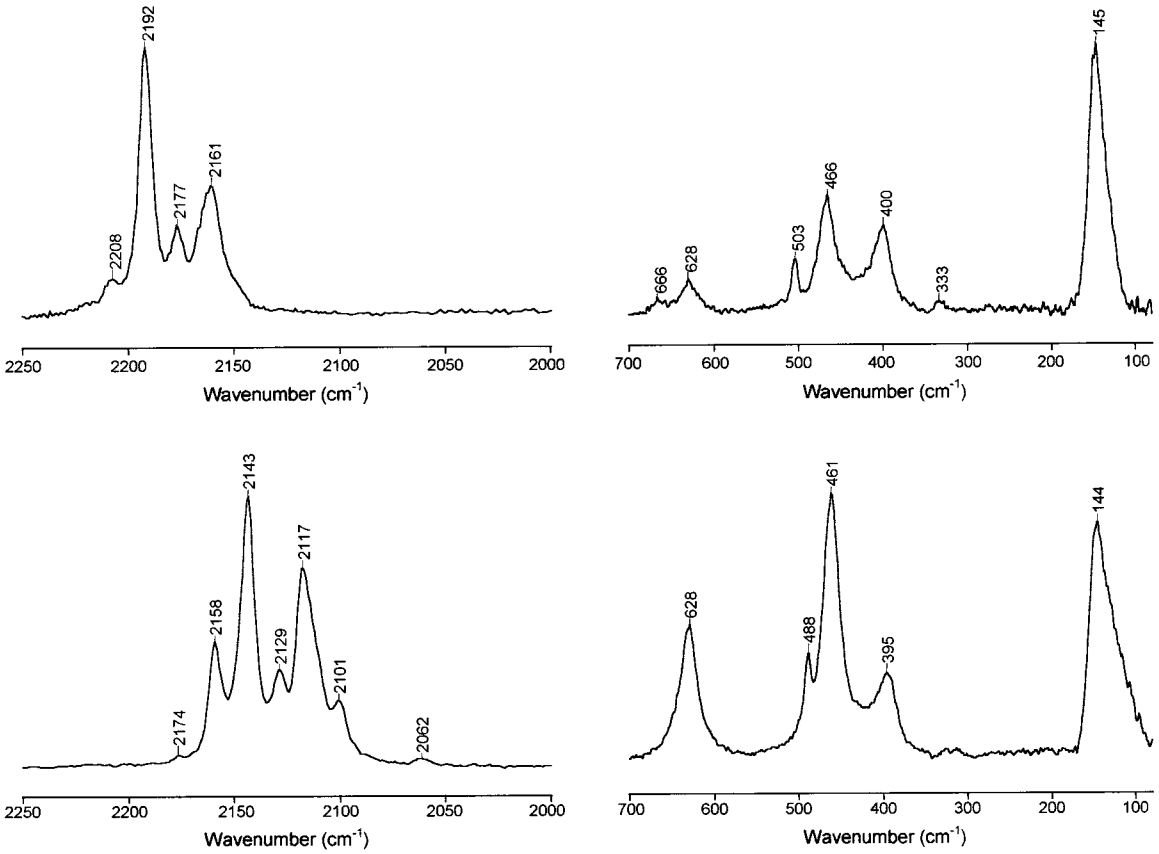

Figure 5. Raman spectra of $[Pt_2(^{12}CN)_{10}]^{4-}$ (upper trace) and $[Pt_2(^{13}CN)_{10}]^{4-}$ (lower trace) complexes in aqueous solution

the $[Pt(CN)_5(H_2O)]^-$ complex gives rise to a broad band at almost the same frequency, 544 cm^{-1}. These stretching frequencies are within the range, between 530 and 580 cm^{-1}, found for Pt−OH stretching frequencies in dichlorodiammine-dihydroxoplatinum (IV) compounds.[31,32]

2.3. Pt−C Stretching Vibrations. These vibrations belong to similar symmetry species as the CN stretching modes. However, the assignment is more difficult because they are weaker and broader than the CN stretchings and also overlapped by the Pt−C−N linear bending modes.

There should be two major Raman bands in this region for the solution spectra. One polarized band around 465 cm^{-1} should arise from the symmetric PtC stretches in the equatorial plane (ν_3). The next polarized strong/medium Raman band attributed to Pt−C apical stretching appeared at ~450 cm^{-1} in the solid-state spectra of $[Pt(CN)_5X]^{2-}$ (X = Cl, Br, and I),[18] at ~ 415

TABLE 5: Experimental and Calculated Frequencies of Normal Modes (cm^{-1}) for $[Pt_2(^{12}CN)_{10}]^{4-}$ and $[Pt_2(^{13}CN)_{10}]^{4-}$ [a]

$[Pt_2(^{12}CN)_{10}]^{4-}$		$[Pt_2(^{13}CN)_{10}]^{4-}$			
experimental	calculated	experimental	calculated	symmetry species	description of normal mode[a]
2192	2192.5	2143	2142.5	A_{1g} (ν_1)	CN stretching modes in equatorial plane
	2192.5		2142.5	A_{2u}	
2185	2183.8	2134	2134.0	B_{1g}	
	2183.8		2134.0	B_{2u}	
2177	2170.8	2128	2123.0	E_g	
	2170.8		2123.0	E_u	
2161	2160.5	2117	2112.7	A_{1g} (ν_2)	Axial CN stretchings
	2160.5		2112.7	A_{2u}	
466	468.1	461	460.4	A_{1g} (ν_3)	PtC equatorial stretchings
	468.1		460.4	A_{2u}	
471	468.2	461	460.5	B_{1g}	
	468.2		460.5	B_{2u}	
429	421.5	411	414.8	E_g	
	417.5		414.8	E_u	
400	401.4	395	394.8	A_{1g} (ν_4)	PtC axial stretchings
	398.9		392.3	A_{2u}	
503	508.4	488	491.0	A_{1g} (ν_5)	PtCN linear bending perpendicular to equatorial plane (ϵ)
	508.4		491.0	A_{2u}	
	453.1		451.4	B_{2u}	
	453.1		451.4	E_u	
446	447.8	443	439.3	E_g	
333	332.1	318	321.7	B_{1g}	
	398.4		387.0	E_u	PtCN axial linear bendings (ϵ_a)
400	397.5	395	386.4	E_g	
477	466.1	461	458.1	E_g	PtCN linear bendings in equatorial plane (ϵ')
	453.1		453.3	A_{2g}	
	436.5		433.7	E_u	
333	332.1	320	321.7	B_{1g}	
	332.1		321.7	B_{2g}	
	332.1		321.7	B_{1u}	
145	145.3	144	144.9	A_{1g} (ν_6)	Pt−Pt stretchings

[a] In addition, the 18 calculated skeletal deformation modes (CPtC and PtPtC) are $[Pt_2(^{12}CN)_{10}]^{4-}$, 2 × 127, 2 × 109, 2 × 106, 88, 2 × 84, 2 × 76, 2 × 75, 69, 2 × 60 and 2 × 43 cm^{-1}; $[Pt_2(^{13}CN)_{10}]^{4-}$, 2 × 126, 2 × 108, 2 × 106, 88, 2 × 84, 2 × 76, 2 × 74, 68, 2 × 59 and 2 × 43 cm^{-1}; totally 59 normal modes (27 single and 16 double degenerate vibrations, the torsional mode not included).

TABLE 6: Calculated CN Stretching Frequencies for Different ^{13}CN Labeled Species[a]

		$[Pt_2(^{12}CN)_{10}]^{4-}$			$[Pt_2(^{13}CN)_{10}]^{4-}$		
assignments[b]		$(^{12}CN)_{10}$	$^{13}CN_{eq}$ $(^{12CN})_9$	$^{13}CN_{ax}(^{12}CN)_9$	$(^{13}CN)_{10}$	$^{12}CN_{eq}(^{13}CN)_9$	$^{12}CN_{ax(}{}^{13CN)}{}_9$
equatorial	A_{1g}	2192.5	2192.5	2192.5	2142.5	2142.5	2142.5
	A_{2u}	2192.5	*2189.7*	2192.5	2142.5	*2138.6*	2142.5
	B_{1g}	2183.8	2183.8	2183.8	2134.0	2134.0	2134.0
	B_{2u}	2183.8	*2179.4*	2183.5	2134.0	*2128.7*	2134.0
	E_g	2170.8	*2129.2*	2170.8	2123.0	*2181.1*	2123.0
	E_u	2170.8	2170.8	2170.8	2123.0	2123.0	2123.0
axial	A_{1g}	2160.5	2160.5	2160.5	2112.7	2112.7	2112.7
	A_{2u}	2160.5	2160.5	*2112.7*	2112.7	2112.7	*2160.5*

[a] Large isotopic shifts are in italics. [b] Symmetry species in ideal D_{4h} point group symmetry.

cm^{-1} for aqueous solutions of the dimetallic Pt−Tl complexes,[12] and was observed at 400 cm^{-1} for the $[Pt_2(CN)_{10}]^{4-}$ complex. Both Raman spectra of the $[Pt(CN)_5(H_2O)]^-$ and $[Pt(CN)_5(OH)]^{2-}$ complexes exhibit only one rather broad and medium intensity band at 466 and 463 cm^{-1}, respectively. There is no second major band in this region, though on the low-frequency side of the broad bands, a weak shoulder is apparent. The shoulder at 439 cm^{-1} for $[Pt(CN)_5(OH)]^{2-}$ seems to be polarized. Therefore, we assigned this feature to the axial A_1 stretching mode (ν_4). The B_1 $Pt-C_{eq}$ stretching mode has been observed in the 455−470 cm^{-1} spectral range for $[Pt(CN)_5X]^{2-}$ (X = Cl, Br, and I)[18] and for the $[(NC)_5PtTl(CN)_n]^{n-}$ (n = 1, 2, and 3),[12] $[Pt(CN)_4Cl_2]^{2-}$, and $[Pt(CN)_4]^{2-}$complexes.[33,34] According to the above considerations, the B_1 vibration (ν_{10}) around 460 cm^{-1} may also be assigned to the A_1 (ν_3) mode.

The assignment of the asymmetric E mode (ν_{16}) is not possible because in the 410−420 cm^{-1} region no bands have been observed. For force constant calculations, we have adopted an average frequency at 418 cm^{-1} as the ν_{16} mode.[12,18]

2.4. Pt−C−N Deformations. The out-of-plane (coordinate ϵ in Figure 6) linear bendings give rise to the A_1 (ν_6), B_1 (ν_{11}), and E (ν_{17}) species. The weak polarized lines at 502 and 485 cm^{-1} were assigned to the "umbrella" mode of Pt−CN deformation of the A_1 symmetry species for the $[Pt(CN)_5(H_2O)]^-$ and $[Pt(CN)_5(OH)]^{2-}$ complexes, respectively.

According to this assignment, the general trend for the A_1 species has been preserved, that is, $\nu_6 > \nu_3 > \nu_4$. The relative closeness of the other two deformational modes, ν_{11} and ν_{17}, suggested an assignment to the weak band around 440 cm^{-1}, which also was ascribed to the PtC stretching mode ν_4.

Because the A_2 (ν_8) in-plane PtCN deformation is inactive, only two Raman active vibrations can be expected, namely, B_2 (ν_{13}) and E (ν_{18}). According to the normal coordinate calculations, the ν_{18} frequency should occur below 400 cm^{-1}. There-

TABLE 7: Raman Frequencies from the $[Pt(CN)_5(H_2O)]^-$ and $[Pt(CN)_5(OH)]^{2-}$ Complexes in Aqueous Solution

$[Pt(CN)_5(H_2O)]^-$			$[Pt(CN)_5(OH)]^{2-}$			
band position (cm^{-1})	rel intensity	depolarization ratio	band position (cm^{-1})	rel intensity	depolarization ratio	assignment[a]
2207	100	0.03	2202	100	0.03	CN symm. stretch equatorial
2196	45	0.71	2190	31	0.69	CN asymm. stretch equatorial
2194	vw, sh		2176	vw sh		CN stretch axial
2167	6	0.02	2167	8	0.02	$[Pt(CN)_4]^{2-}$ impurity
2148	2	0.77	2148	3	0.74	
630	27	0.74				ClO_4^- band (ν_4, F_2)
			580	4		
			546	31	0.23	Pt−OH stretch
544	6					Pt−OH_2 stretch
502	15	0.12	485	8	0.38	PtCN linear bending
466	70	0.38	463	54	0.27	Pt−C symm. stretch equatorial
441	13, sh		439	14	0.41	Pt−C asymm. stretch equatorial, axial
334	1		∼330	vvw		PtCN linear bending
			175	5		CPtC deformation
			118	8	0.24	CPtC deformation

[a] Tentative assignment based on refs 12, 18, and 34. Abbreviations for intensity are w, weak; v, very; and sh, shoulder.

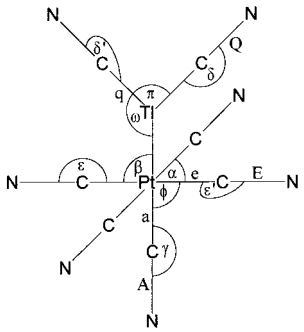

Figure 6. Types of internal coordinates for the $[(NC)_5PtX]^{2-}$ complexes. Additional features are ρ and χ for wagging and torsional modes of X = Tl−C_2 and Tl−C_3 groups, respectively.

fore, the very weak Raman feature around 330 cm^{-1} was assigned to the E (ν_{18}) species. The B_2 (ν_{13}) vibration was found in the range of 421−435 cm^{-1} for the $[Pt(CN)_5X]^{2-}$ (X = Cl, Br, and I) complexes;[18] therefore, the bands around 440 cm^{-1} which have the lowest frequency in the 400 cm^{-1} region were assigned to this ν_{13} mode.

No observed band in the 400 cm^{-1} region could be assigned to the doubly degenerate linear bending of the apical PtCN group (ν_{14}). In accordance with the normal coordinate calculations and assignment of the $[(NC)_5PtTl(CN)_n]^{n-}$ (n = 1, 2 and 3) complexes,[12] the ν_{19} mode was ascribed a vibrational frequency of 410 cm^{-1}.

2.5. C−Pt−C and O−Pt−C Deformations. The Raman spectrum of the $[Pt(CN)_5(OH)]^{2-}$ solution showed a depolarized band at 175 cm^{-1} and a band at 118 cm^{-1} (probably polarized). The latter can be assigned to the A_1 symmetric CPtC bending mode (ν_7). The normal coordinate calculations indicate that a reasonable assignment of the band at 175 cm^{-1} is as ν_{20}, the E mode of the CPtC deformation. The E (ν_{21}), B_2 (ν_{11}), B_1 (ν_{12}), and E (ν_{22}) modes were tentatively ascribed to calculated frequencies at 143, 118, 74, and 75 cm^{-1}. The assignments of 22 fundamental modes are summarized in Table 8.

Force Constant Calculations. The general problem in this type of calculation is the limited number of experimental frequencies. This problem partly originates from the specific nature of IR and Raman spectra of aqueous solutions. Additional support for the assignments discussed above can be obtained in Figure 7. The PtC stretching and PtCN linear bending modes of pentacyanoplatinum complexes are clearly separated into two groups.[12,18] The ν_3, ν_6, ν_{10}, ν_{11}, and ν_{17} bands are found between 460 and 490 cm^{-1}, and the ν_4, ν_{13}, ν_{16}, ν_{18} and ν_{19} fundamentals are found around 420 cm^{-1}. These two sets correspond to the two broad experimental Raman features at 466 and at around 400 cm^{-1} of $[Pt_2(CN)_{10}]^{4-}$ in this region (Figure 5). Note that the low-frequency band has moved down about 10−15 cm^{-1} for the dimetallic complex as compared to the reference $[Pt(CN)_5X]^{2-}$ (X = Cl, Br, and I) complexes.[18] This explains the poor agreement in band positions for the group of low frequency fundamentals. These two bands are used as approximate experimental frequencies for the two groups of fundamentals. These approximations will have little influence on the major stretching force constants, especially for series of complexes with similar structures.

Previously, it was shown that in order to obtain an accurate value of the metal−metal stretching force constant the ligands must be accounted for in the vibrational analysis.[12] Despite the limited number of observed vibrational frequencies, a normal coordinate analysis was performed for the $[(^{12}CN)_5Pt-Pt(^{12}CN)_5]^{4-}$ and $[(^{13}CN)_5Pt-Pt(^{13}CN)_5]^{4-}$ complexes, using reasonable assumptions of the force field and the interaction constants. These were based on previous results from normal coordinate analyses of the $-Pt(CN)_5$ unit. The basic assumptions are the following: 1. Free rotation around the Pt−Pt bond, giving no difference in calculated frequencies for D_{4d} (staggered) and D_{4h} (eclipsed) configuration. 2. Very weak coupling between the C−N and Pt−C frequencies of the two $-Pt(CN)_5$ units of the molecule. This means that the totally symmetric Raman modes (A_{1g}) can be used as a good approximation also for the frequencies of the A_{2u} modes, which are the out-of-phase symmetric vibrational modes.

Only a small separation occurs between the symmetric and asymmetric Pt−C_{ax} stretching frequencies along the linear NC−Pt−Pt−CN unit, when no specific interaction force constants are introduced, implying weak coupling between these modes. The number of observed frequencies (Table 4) allowed refinements only of force constants for normal modes belonging to the A_{1g} and A_{2u} symmetry species. The remaining force constants had to be constrained, and as the starting force field, we have used that of the dimetallic $[(NC)_5Pt-Tl(CN)_2]^{2-}$ complex, cf. Table 9.

Our basic strategy was to assign all possible CN and PtC stretching modes to fit the most important stretching force constants for the major chemical bonds. In that process, we were carefully testing the effects that lacking frequencies and possible differences in the assignments would have on the force constant

TABLE 8: Assigned Experimental Normal Modes (cm^{-1}) and Calculated Potential Energy Distributions (PED) for the $[Pt(CN)_5(H_2O)]^-$, $[Pt(CN)_5(OH)]^{2-}$, and $[Pt(CN)_5I]^{2-}$ Complexes[a]

C_{4v}[b]	no.	approximate description of modes[c]	$[Pt(CN)_5(H_2O)]^-$	$[Pt(CN)_5(OH)]^{2-}$	$[Pt(CN)_5I]^{2-}$	P.E.D. (%)[d]
A_1	ν_1	CN str (eq)	2207	2202	2199.5	94E + 6e
	ν_2	CN str (ax)	2194	2176	2191	96A + 4e
	ν_3	PtC str (eq)	466	463	467	94e + 6E
	ν_4	PtC str (ax)	441	439	432.9	91a + 4A + 3ϵ
	ν_5	PtO str, PtI str	544	546	180.6	88m + 7ϵ + 4a + 2$\beta\varphi$
	ν_6	PtCN def (eq)	502	485	467	77ϵ + 12$\beta\varphi$ + 10m + 1a
	ν_7	CPtC def (ap)	(118)[e]	118	107.4	86$\beta\varphi$ + 14ϵ
A_2	ν_8	PtCN def (eq)	441	439	432.9	100ϵ'
B_1	ν_9	CN str (eq)	2199	2190	2187.7	94E + 6e
	ν_{10}	PtC str (eq)	466	463	467	94e + 6E
	ν_{11}	PtCN def (eq)	441	439	432.9	91ϵ + 9$\beta\varphi$
	ν_{12}	CPtC def (ap)	[75][f]	[74]	[74]	91$\beta\varphi$ + 9ϵ
B_2	ν_{13}	PtCN def (eq)	466	463	467	72ϵ' + 28α
	ν_{14}	CPtC def (eq)	118	118	107.4	72α + 28ϵ'
E	ν_{15}	CN str (eq)	2194	2176	2179.5	96E + 4e
	ν_{16}	PtC str (eq)	(418)	(418)	432.9	93e + 4e + 2ϵ' + 1α
	ν_{17}	PtCN def (eq)	441	439	(428)	83ϵ + 17$\beta\varphi$
	ν_{18}	PtCN def (eq)	334	330	342	80ϵ' + 18$\beta\varphi$ + 3e
	ν_{19}	PtCN def (ax)	(410)	(410)	(418)	100γ
	ν_{20}	CPtC def (eq)	(175)	175	[178]	72$\beta\varphi$ + 15ϵ + 13$\beta'\varphi'$
	ν_{21}	CPtC def (ap)	[149]	[143]	[138]	86$\beta'\varphi'$ + 11$\beta\varphi$ + 2ϵ
	ν_{22}	OPtC def (ap), IPtC def (ap)	[77]	[75]	[69]	81α + 18ϵ' + 1$\beta'\varphi'$

[a] Experimental data for $[Pt(CN)_5I]^{2-}$ from ref 18. [b] Symmetry species for point group C_{4v}, with H_2O and OH considered as point masses. [c] (eq) equatorial; (ax) axial; and (ap) apical. [d] P.E.D. as obtained for $[Pt(CN)_5(OH)]^{2-}$. The P.E.D.s for the $[Pt(CN)_5(H_2O)]^-$ and $[Pt(CN)_5I]^{2-}$ complexes are similar. [e] Experimental frequencies adapted from analogue molecules are given within rounded brackets. [f] Calculated frequencies are given in square brackets. Unobserved experimental frequencies for skeletal bending and torsional modes are expected below 120 cm^{-1}.

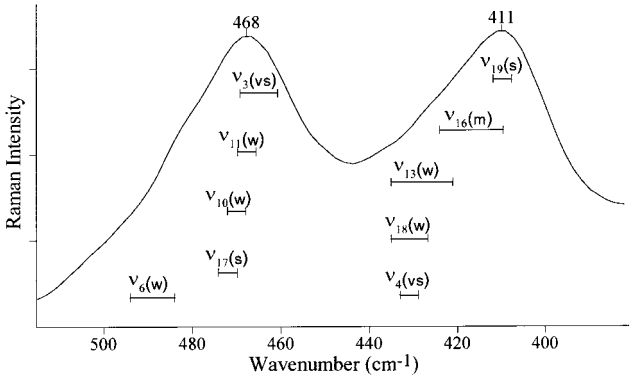

Figure 7. Raman trace of $[(NC)_5Pt-TlCN]^-$ in aqueous solution between 400 and 500 cm^{-1} in the PtC stretching and PtCN linear bending regions. The insets show the observed spectral ranges for fundamentals of solid $M_2[Pt(CN)_5X]$ compounds, where M = Na, K, and Cs and X = Cl, Br, and I (for the numbering of the fundamentals, cf. Table 8). [12]

calculations. For the equatorial CN stretching modes, two bands at 2192 and 2177 cm^{-1} can be clearly observed as the A_{1g} and E_g species. If these values are used for the $[Pt_2(^{12}CN)_{10}]^{4-}$ complex, and likewise 2143 and 2128 cm^{-1} for $[Pt_2(^{13}CN)_{10}]^{4-}$ without refining the unobserved B_{1g} frequencies, the CN stretching force constant gets the value 1712 N m^{-1} when constraining the interaction terms to values adopted from similar molecules, i.e., 6 and 3 Nm^{-1} for the cis and trans interactions, respectively. When three experimental frequencies, 2192 (2143), 2185 (2134), and 2177 (2128) cm^{-1}, are used for the ^{12}CN (^{13}CN within brackets) modes, the CN stretching force constants become +1718, −10.2, and +3.1 N m^{-1} (cf. Table 9), which is rather close to the former restricted solution.

A similar procedure can be performed for the Pt−C stretching force constants. A refinement based on only two pairs of experimental frequencies, namely, 466 (461) and 429 (411) cm^{-1} for the ^{12}CN (^{13}CN in brackets) complexes, gives the value 283.5 N m^{-1} for the Pt−C stretching force constant. The trans and cis interaction terms were in this case constrained to 66 and 2 N m^{-1}. A calculation based on all experimental data, namely, three pairs (A_{1g}, B_{1g}, and E_g) of frequencies (Table 5), lead to the Pt−C equatorial stretching force constants 287.4, 69, and 0.0 N m^{-1} (Table 9), again rather close to the constrained solution.

It can be concluded that the fundamental problem in the present situation, the difficulties in assignments and restrictions in the number of observed experimental frequencies, can be handled by constraining some minor interaction terms to reasonable values and refining only the main force constants (the diagonal values in the matrixes). In this way, we do not use assumed fundamental frequencies as basic input for force constant refinements and can assess the accuracy of the resulting values. After carefully considering the approximations discussed above, the calculated fundamental frequencies listed in Tables 5 and 6 gave an important support for the assignment and improved the understanding of the vibrational properties of the $[Pt_2(CN)_{10}]^{4-}$ complex.

The stretching force constants of the mononuclear $Pt(CN)_5$ derivatives were obtained by means of a similar treatment. Experimental fundamental frequencies recorded for the $[Pt(CN)_5I]^{2-}$ complex in aqueous solution were taken from ref 18. The assigned Raman frequencies (Table 7) and selected fundamental modes (Table 8) have been used to refine force constants for the $[Pt(CN)_5(H_2O)]^-$, $[Pt(CN)_5(OH)]^{2-}$, and $[Pt(CN)_5I]^{2-}$ complexes, cf. Table 9. The agreement between experimental and calculated stretching frequencies was within a few wavenumber units in most cases. The PtCN linear bendings and skeletal deformational force constants were constrained in all calculations, because of the weak experimental support for the low-frequency modes below 150 cm^{-1}.

Discussion

Pt−Pt Bond Distances and Other Dimeric Cyano Complexes. A number of compounds have been found with partially oxidized columnar chains of stacked square planar $Pt(CN)_4$

TABLE 9: Force Constants for $[Pt(CN)_6]^{2-}$, $[Pt(CN)_5(H_2O)]^{-}$, $[Pt(CN)_5(OH)]^{2-}$, $[Pt(CN)_5I]^{2-}$, $[(NC)_5Pt-Tl(CN)_n]^{n-}$ (n = 1, 2, and 3), and $[Pt_2(CN)_{10}]^{4-}$ Complexes[a]

force constants	coord involved	$[Pt(CN)_6]^{2-}$	$[Pt(CN)_5(H_2O)]^{-}$	$[Pt(CN)_5(OH)]^{2-}$	$[Pt(CN)_5I]^{2-}$	$[(NC)_5Pt-TlCN]^{-}$	$[(NC)_5Pt-Tl(CN)_2]^{2-}$	$[(NC)_5Pt-Tl(CN)_3]^{3-}$	$[(NC)_5Pt-Pt(CN)_5]^{4-}$	unit
				Stretchings						
K(CN), equatorial	E	1743	1756	1736	1733	1736	1730	1718	1717	a
f(CN, CN) trans	E, E	−4.7	−13.9	−4.0	−8.5	−4.5	−3.8	−3.4	−10.2	a
f(CN, CN) cis	E, E	2.7	3.2	4.8	5.2	3.1	4.1	4.7	3.1	a
K(CN) axial	A	1743	1755	1722	1750	1735.6	1722	1719	1710	a
K(CN), Tl	Q					1750	1723	1739		a
f(CN, CN), Tl	QQ						7.9	−4.6		a
K(PtC), equatorial	e	294.3	282.3	281.3	288.8	276.5	282.3	281.1	287.4	a
f(PtC, PtC) trans	e,e‘	64.9	68.1	67.1	64.4	66.7	66.4	66.7	69.0	a
f(PtC, PtC) cis	e,e	2.9	0.5	0.2	0.2	2.4	0.0	0.0	0.0	a
K(PtC) axial	a	294.3	261.9	271	262.6	238.1	239.6	242.8	227.1	a
K(TlC)	q					188.8	180.9	166.4		a
f(TlC, TlC)	qq						−21.0	22.5		a
K(PtTl), K(PtPt), K(PtO), K(PtI)	m		268.6	264.1	191.4	173.6	169.3	156.3	123.8	a
				Bendings						
H(PtC_2) equatorial	α	49.3	(34)	(34)	(34)	(33)[c]	(33)[c]	(33)[c]	(34)	b
h(PtC_2 PtC_2)	αα	−2	(−14)	(−14)	(−14)	(−15)	(−15)	(−15)	(−14)	b
H(MM′C), H(OPtC)	β		(34)	(34)	(34)	(34)	(34)	(34)	(34)	b
h(MM′C, MM′C)	$\beta\beta$		(−8)	(−8)	(−8)	(−8)	(−8)	(−8)	(−8)	b
h(XPtC, XPtC)[d]										
H(PtC_2) axial	φ		(34)	(34)	(34)	(34)	(34)	(34)	(34)	b
h(PtC_2, PtC_2)	$\varphi\varphi$		(−8)	(−8)	(−8)	(−8)	(−8)	(−8)	(−8)	b
H(PtTlC)	ω					(30)	(13)	(19)		b
H(TlC_2)	π						(46)	(10)		b
h(PtTlC, PtTlC)	$\omega\omega$					−	0	(3)		b
h($TlC_{2,TlC2}$)	$\pi\pi$					−	0	(3)		b
				Linear bendings						
H(PtCN) equatorial	ϵ	45.3	50.7	49.4	53.3	48.1	47.4	46.9	47.8	b
h(PtCN, PtCN) trans	$\epsilon\epsilon$	7.7	5.8	1.2	5.0	4.8	5.8	6.5	(5)	b
h(PtCN, PtCN) cis	$\epsilon\epsilon$	2.7	3.6	0.5	−1.3	0	0	0	0	b
H'(PtCN) equatorial	ϵ'	45.3	37.9	37.6	38.5	40.4	41.0	42.8	39.7	b
h'(PtCN, PtCN) trans	$\epsilon'\epsilon'$	7.7	12.3	12.3	11.0	13.5	14.1	15.8	(14)	b
h'(PtCN, PtCN) cis	$\epsilon'\epsilon'$	2.7	2.5	2.6	1.7	−3.2	−1.7	−1.2	(0)	b
H(TlCN)	δ	−				19.8	16.2	19.3		b
h(TlCN, TlCN)	δ,δ	−				−	−3.9	−0.5		b
H'(TlCN)	δ'	−				(19.8)	19.2	23.2		b
h'(TlCN, TlCN)	δ',δ'	−				−	1.4	−1.2		b
H(PtCN) axial	γ	45.3	46.7	47.1	48.8	42.6	43.0	45.6	44.0	b
				Torsional modes						
χ(CPtTlC)	χ	-				-	(0.10)	(12)	-	b
ρ($PtTlC_2$)	ρ	-				-	(0.20)	-	-	b

[a] K, stretching; H, bending; ρ and χ, torsional and diagonal; and f, stretch−stretch and h, bend−bend interaction terms. [a] Unit: N m^{-1}. [b] Unit: 10^{-16} N m. [c] The constrained values are in brackets. [d] Apical substituent (X = H_2O, OH, or I) for mononuclear complexes.

groups.[2] In the $M_2[Pt(CN)_4X_{0.25-0.40}]$ compounds, where M is a univalent cation and X = Cl and Br, relatively short Pt−Pt distances (<3 Å) occur, again with little change in the Pt−C bond distances. The shortest Pt−Pt distance, 2.798(1) Å, is found for the $Rb_2[Pt(CN)_4](FHF)_{0.40}$ compound, for which the formal oxidation state of platinum is 2.4.[35]

The torsion angle between adjacent planar $Pt(CN)_4$ groups is found to be correlated to the Pt−Pt distance. The eclipsed conformation with parallel cyano ligands for large separations (over about 3.7 Å) gradually transforms to a completely staggered one at about 2.9 Å, because of the increasing $\pi-\pi$ repulsion between the cyano groups.[36] Thus, the short Pt−Pt bond distance, 2.73(1) Å, for the singly bonded $[Pt_2(CN)_{10}]^{4-}$ complex shows that the complex should be in a staggered conformation (cf. Figure 4). However, for other symmetrically ligand-bridged diplatinum(III) complexes, considerably shorter Pt^{III}-Pt^{III} distances are found, in the range of 2.39−2.58 Å.[1,37,38] The structures indicate strain and repulsion between the platinum atoms, and it was suggested that Pt−Pt distances close to 2.46 Å as in the sulfate bridged dimers are close to optimum for O-donor ligands.[38]

For a single unhindered $Cl-Pt^{III}-Pt^{III}-Cl$ bond, the typical Pt−Pt distance is 2.70 Å.[6,7] For the $[Pt_2Cl_6HN{=}C(OH)C(CH_3)_{34}]$ complex with chloride atoms both in equatorial (cis) and axial (trans) positions, the much longer $Pt-Cl_{ax}$ bond distance indicates a strong trans influence by the $Pt^{III}-Pt^{III}$ bond.[7] A similar bonding situation with pronounced σ character of the metal−metal bond is also indicated by the metal−ligand interactions in $[(NC)_5Pt-Pt(CN)_5]$,$^{4-}$ for which the spin−spin coupling constant $^1J(Pt-C_{trans})$ is much smaller than $^1J(Pt-C_{cis})$. This indicates strong trans influence (ref 12, Table 1), keeping in mind that both the Pt−CN bond strength and the amount of s-electron contribution will influence these constants.

The Pt−Pt bond in the Pt_2^{6+} entity is usually regarded to have a $\sigma^2\pi^4\delta^2\delta^{*2}\pi^{*4}$ molecular orbital configuration.[1,38] A closely related analogous isoelectronic d^7d^7 system is provided by the $[Co_2(CN)_{10}]^{6-}$ complex in the $Ba_3[Co_2(CN)_{10}]\cdot 13H_2O$ salt.[39,40] The axial Co−CN bond distances are significantly longer than the equatorial, indicating a trans effect of the Co−Co metal−metal bond. The complex has a close to staggered conformation of the two $Co(CN)_5$ groups. Even though the Co−Co distance, 2.796 Å, is longer than the Pt−Pt distance, 2.726-

(3) Å, obtained in the present work, it has been suggested that the limiting factor for the Co−Co single bond distance is the repulsion between nonbonding halves of the dimer.[40] However, in the $[Mo_2(CN)_8]^{4-}$ complex, the quadruple Mo−Mo bond keeps the cyano ligands in eclipsed conformation in a square pyramidal coordination geometry. There is strong repulsion between the cyano ligands on the neighboring Mo atoms because of the very short Mo−Mo bond distance, 2.122(2) Å, giving slightly bent cyano ligands with Mo−C−N angles of 173−175°.[41]

The 18-Electron Rule and Cyano Complexes. This electron-counting rule accounts for the fact that many stable transition metal compounds have coordination numbers such that the metal atom has 18 electrons available for its nine valence orbitals. It is a useful qualitative model for rationalizing the structures of many low-valent organometallic complexes, in particular carbonyl complexes, but it is violated in a wide variety of other complexes.[16] The predicting power of such simplifying rules is often limited as the outcome depends on a number of balancing factors for the orbital interactions, such as availability of ligand orbitals for σ-bonding, relativistic contraction of metal orbitals, π-back-bonding, and coordination geometry. Moreover, charge and steric effects are important, and the repulsion between the cyano ligands in the two connected $-Pt^{III}(CN)_5$ units in octahedral coordination geometry must be considered. However, we find that the 18-electron rule can be useful for rationalizing the structure and bonding also in metal−cyano complexes.

The cyano and carbonyl ligands have many properties in common, even though the cyano ligand is a stronger σ donor and a weaker π acceptor because of its negative charge.[41] For octahedral cyano complexes, the valence shell s, p, and d_{z^2} and $d_{x^2-y^2}$ orbitals of the metal atom combine with a symmetry allowed linear combination of six σ orbitals from the ligands.[42,43] Group theory shows that the six σ-bonding molecular orbitals belong to the a_{1g}, t_{1u}, and e_g symmetry species in the O_h point group. The low-energy antibonding cyano ligand π^* orbitals can accept electron density from the three remaining metal atom d orbitals (d_{xy}, d_{xz}, and d_{yz}) of t_{2g} symmetry, which then become weakly bonding. This also increases the energy gap between the weakly antibonding $t_{2g}^*-e_g^*$ MOs dominated by the metal atom (Δ_{oct} in ligand field theory, see, e.g., Figure 7.17 of ref 42). The interacting valence electrons of the complex will then in this octahedral MO scheme preferably fill these nine bonding orbitals, as, e.g., for the $[Pt(CN)_6)]^{2-}$ complex. Remaining electrons from the valence shell of the ligands will occupy the nonbonding t_{1g} and t_{2u} orbitals and also the weakly antibonding t_{2g}^* but not the antibonding e_g^* orbital.[42] Clearly, π-back-bonding is an important reason why the 18-electron rule is favored for the strongly π-accepting isoelectronic cyano, carbonyl, and nitrosyl ligands.

The cyano complexes of platinum are found in several oxidation states. Well-known for d^8 metal atoms are the 16-electron square planar cyano complexes $[M^{II}(CN)_4]^{2-}$, M = Ni, Pd, and Pt. An MO diagram shows that the 16 electrons will all occupy bonding MOs and that the nonbonding occupied d_{z^2} orbital on the metal atom would repel additional axial ligands.[43] However, with a change of coordination geometry, the addition of another cyano ligand would lead to a five-coordinated 18-electron complex. No such cyano complex has been found for platinum(II), but for nickel(II), five-coordinated $[Ni(CN)_5]^{3-}$ complexes are known both in trigonal bipyramidal configuration and in square pyramidal geometry,[41] certainly an effect of the lower penetration into the valence shell of the 3d orbitals.

The isolated 17-electron square pyramidal $[Co^{II}(CN)_5]^{3-}$ complex exists,[41] but neither $[Pt^{III}(CN)_5]^{2-}$ nor $[Ni^{III}(CN)_5]^{2-}$ has been found. However, a single two-electron Pt−Pt bond between two $Pt^{III}(CN)_5$ units satisfies the 18-electron count as in the currently studied $[Pt^{III}_2(CN)_{10}]^{4-}$ complex. Can similar $[M_2(CN)_{10}]^{n-}$ complexes conforming to the 18-electron rule form with the other members of group 9 and 10, Rh(II), Ir(II), Ni(III), and Pd(III)? It seems likely that the hitherto unobserved metal−metal bonded $[Pd_2(CN)_{10}]^{4-}$ as well as $[Rh_2(CN)_{10}]^{6-}$ and $[Ir_2(CN)_{10}]^{6-}$ complexes could exist with similar octahedral coordination as in the isoelectronic $[Pt_2(CN)_{10}]^{4-}$ and $[Co_2(CN)_{10}]^{6-}$ species. However, the shorter metal−metal bond length for a $[Ni^{III}_2(CN)_{10}]^{4-}$ complex will increase the steric strain from ligand-ligand repulsion, and destabilize octahedral coordination geometry.

The existence in aqueous solution of dimeric $[Fe_2(CN)_{10}]^{n-}$ (n = 4, 5, or 6) complexes has been known for a long time.[43] In these cases, a metal−metal bond is not consistent with the 18-electron rule, and a double cyano bridge between the metal atoms was proposed.

In a tetrahedral coordination geometry with π-accepting ligands, the metal d−p orbitals can mix both in the σ and π bonds. Besides the four σ-bonding a_1 and t_2 MOs, there will be five π-bonding e and t_2 MOs (cf. Figure 7.19 of ref 42), and, e.g., the tetrahedral $[Tl(CN)_4]^-$ complex will then be surrounded by 18 bonding valence electrons. When we mixed in solution the 16-electron $[Pt(CN)_4]^{2-}$ complex with the 18-electron $[Tl(CN)_4]^-$ complex, a single metal−metal bond formed giving a $[(CN)_5Pt-Tl(CN)_3]^{3-}$ complex.[10] Now both metal centers follow the 18-electron rule, and the Pt−Tl bond distance is shorter than Pt−Pt in $[Pt_2(CN)_{10}]^{4-}$, 2.64(1) and 2.73(1) Å,[12] respectively. This is consistent with the lower ligand−ligand repulsion between the octahedral Pt and tetrahedral Tl centers in the $[(CN)_5Pt-Tl(CN)_3]^{3-}$ complex and is reflected in the M−M stretching force constant, 156 Nm^{-1}, which is larger than that for $[Pt_2(CN)_{10}]^{4-}$, 124 Nm^{-1} (Table 9).

How useful is the 18-electron rule for cyano complexes in general? Obviously, with single bonds and d^{10} ions, the 18-electron rule requires the coordination number four and is not fulfilled for some strongly covalent cyano complexes, e.g., $[Au(CN)_2]^-$ and $[Hg(CN)_2]$.[41] Even when we restrict our considerations to pure and isolated cyano complexes, many can be found with a formal count of less than 18 valence electrons around the metal atom, as in the homologous series of $[M^{III}(CN)_6]^{3-}$ complexes from Cr to Co with steadily decreasing M−C bond length.[41] Nevertheless, numerous five-, six-, seven-, and eight-coordinated cyano complexes favor the 18-electron count, although for eight coordination and d^1 and d^2 metal atoms, e.g., for Mo, W, and Nb, both 17- and 18-electron complexes are common.[41] Evidently, the energy differences are low when filling higher bonding orbitals in many coordination geometries, and the negative cyano ligand makes the charge of the complex an important balancing factor. However, no pure cyano complex seems to exist for which the 18-electron count is exceeded, a common occurrence with more weakly coordinating ligands.

Structure of Mononuclear Platinum(IV) Complexes. Precisely determined Pt−O(H) distances, in the range of 1.99−2.01 Å, were found previously for dichlorodiamminedihydroxoplatinum(IV) compounds.[31,32] They are slightly shorter (~0.03 Å) than the present Pt−O(H) distance, 2.027(7) Å, as can be expected from the influence of the strongly coordinating cyano ligands in the $[Pt(CN)_5(OH)]^{2-}$ group. Also the Pt−O distances in the $(NH_4)_2[Pt(OH)_6]$ and $K_2[Pt(OH)_6]$ salts, 2.017(7) and 2.016(8) Å, respectively,[45] seem to be slightly shorter (~0.01

TABLE 10: Charge Dependence of Cyanide Stretching Force Constants

		CN stretching frequencies (cm^{-1})				CN stretch and CN,CN interaction force constant (N $m^{-1)}$				
No.	complex	$\nu_1(A_1)$	$\nu_2(A_1)$	$\nu_9(B_1)$	$\nu_{15}(E)$	$K(CN)_{eq}$	$K(CN)_{axial}$	$f(CN, CN)_{trans}$	$f(CN, CN)_{cis}$	ref
1.	$[Pt(CN)_5H_2O]^-$	2207	2194	2199	2194	1756	1755	−13.9	3.2	a
2.	$[Pt(CN)_5Cl]^{2-}$	2204.9	2195	2192.7	2187	1748	1766	−6.3	3.6	b, c
3.	$[Pt(CN)_5Br]^{2-}$	2203	2193	2191.5	2186	1746	1762	−6.1	2.7	b, c
4.	$[Pt(CN)_5I]^{2-}$	2199.5	2191	2187.7	2179.5	1733	1750	−8.5	5.2	a, b, c
5.	$[Pt(CN)_5(OH)]^{2-}$	2202	2171	2190	2171	1736	1722	−4.0	4.8	a
6.	$[Rh(CN)_5Cl]^{3-}$	2150	2140	2154	2130	1667	1678	2.8	−3.4	c
7.	$[Rh(CN)_5Br]^{3-}$	2148	2137	2143	2128	1660	1673	−0.8	0.2	c
8.	$[Rh(CN)_5I]^{3-}$	2145	2135	2140	2123	1645	1670	0.9	0.2	c
9.	$[Fe(CN)_5(NO_2)]^{4-}$	2089	2068	2064	2060	1555	1567	−1.0	7.5	c

[a] This work. [b] Experimental frequencies taken from refs 18 and 52. [c] Experimental frequencies taken from ref 52.

Å). The presently obtained Pt−I distance, 2.676(2) Å in the $[(NC)_5PtI]^{2-}$ complex (Table 2), is close to previously obtained Pt−I distances. These are between 2.661(1) and 2.663(1) Å in $[PtI_6]^{2-}$ [46] and 2.686 and 2.699 Å in $[Pt(NH_3)_4I_2]^{2-}$ complexes.[47,48]

The mean Pt−C bond length increases only slightly when going from the divalent square-planar $[Pt^{II}(CN)_4]^{2-}$ complex to the tetravalent octahedral $[Pt^{IV}(CN)_6]^{2-}$ species. The interatomic distances for $K_2[Pt(CN)_4]\cdot 3H_2O$ are Pt−C 1.989 (1.985) Å and Pt−N 3.148 (3.149) Å and, for $K_2[Pt(CN)_6]$, Pt−C 2.005 (2.004) Å and Pt−N 3.153 (3.155) Å, from previous crystallographic and EXAFS (within brackets) studies.[12,29,30]

Vibrational Spectra. 1. MC and CN Stretchings. The C−N symmetric (A_1) stretching frequency of the cyano ligands shows a decreasing trend from 2207, 2202, and 2199.5 to 2192 cm^{-1} for the four complexes $[Pt(CN)_5X]^{n-}$, X = H_2O, OH, I, and $Pt(CN)_5$ (Tables 5 and 8), indicating increasing π-back-bonding, when the donor strength of the ligand increases. The same trend was observed for the corresponding force constant F_{11} (A_1 or A_{1g} in symmetry coordinate representation), namely, 1756, 1736, 1733, and 1712 N m^{-1} for the above series of complexes, respectively (Table 9).

The equatorial C−N symmetric stretching (A_{1g}) frequency (2192 cm^{-1}, Table 4) for the $[Pt^{III}_2(CN)_{10}]^{4-}$ complex, is intermediate between those of the $[Pt^{II}(CN)_4]^{2-}$ and the $[Pt^{IV}(CN)_6]^{2-}$ complexes, 2143.5 and 2211 cm^{-1}, respectively,[34,49] but is higher than those found for the partially oxidized compounds, e.g., 2182 cm^{-1} for $K_2[Pt^{II}(CN)_4]Br_{0.33}$.[50]

The equatorial MC and CN stretching force constants reflect the same trend. They are 294 and 1743 N m^{-1} for $[Pt^{IV}(CN)_6]^{2-}$ and 284 and 1712 N m^{-1} for $[Pt^{III}_2(CN)_{10}]^{4-}$ (Table 9). As expected, the higher the oxidation state, the stronger the M−C σ bonding for the same coordination number.[51] The back-donation then increases and consequently the CN bonding becomes weaker. However, a lower coordination number also increases the back donation to the antibonding cyano orbitals. For the square planar $[Pt(CN)_4]^{2-}$ complex the MC and CN force constants are 275 and 1741 N m^{-1}, respectively.[34] Even though the lower oxidation state gives a slightly smaller MC force constant, the higher availability of back-bonding orbitals on the metal gives a virtually equal CN force constant. This is another example that bond stretching force constants provide a better comparison when discussing bond strengths than frequency comparisons. However, care must be taken to compare bonds of similar nature, because the force constant is a measure of the curvature of the potential well near the equilibrium position and not necessarily its depth and the bond energy.[51]

Based on experimental frequencies obtained for aqueous solutions for $[Pt(CN)_5X]^{2-}$, $[Ru(CN)_5X]^{3-}$, and $[Fe(CN)_5(NO_2)]^{4-}$ complexes,[18,52] a simplified CN stretching force constant calculation has been performed on the basis of the effective G-matrix method, EGM.[53] This method is even simpler than the widely used Cotton-Kraihanzel method[54] but produces all stretching force constants without any constraints very close to the results based on a full solution of the vibrational problem. The results of the calculations are presented in Table 10 together with data for the $[Pt(CN)_5(H_2O)]^-$ and $[Pt(CN)_5(OH)]^{2-}$ complexes obtained by rigorous calculations. The CN stretching force constants become in absolute values about 100−80 N m^{-1} higher when the Cotton−Kraihanzel method is used.[52]

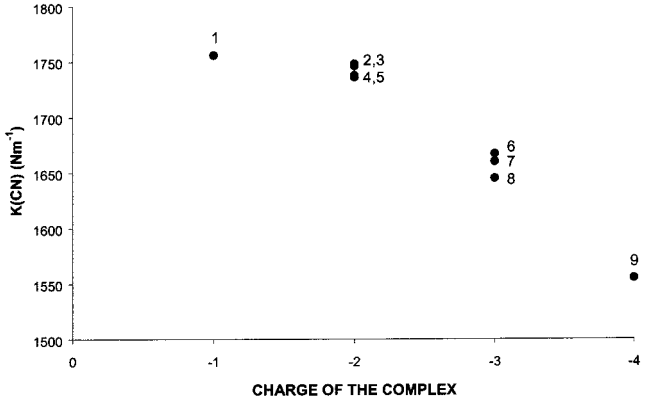

Figure 8. Charge dependence of equatorial CN stretching force constants in pentacyano complexes of heavy metals (cf. Table 10).

An increasing negative charge of the complexes increases the extent of back-donation and, thus, decreases the force constant of the cyano ligand as shown in Figure 8 for the equatorial CN ligands. Both the equatorial and axial CN stretching force constants decrease: 1756/1755 > 1736/1722 > 1712/1710 N m^{-1} for $[Pt(CN)_5(H_2O)]^-$, $[Pt(CN)_5(OH)]^{2-}$, and $[Pt_2(CN)_{10}]^{4-}$, respectively.

For the dimetallic $[(NC)_5Pt-Tl(CN)_n]^{n-}$ (n = 1, 2, and 3) series, the decrease of the K(CN) bond stretching force constant in the $Pt(CN)_5$ unit is more moderate when the negative charge of the complex increases (Table 9). This is certainly due to the special nature of the Pt−Tl bond. The chemical shifts of the ^{195}Pt and ^{205}Tl NMR spectra change in opposite directions which implies a backtransfer of electron density from the $-Tl(CN)_n$ group to platinum when the number of cyano ligands n increases.[10] The intermediate complex (n = 2) has the lowest CN stretching force constant. This is possibly due to a change in coordination number because of hydration of the thallium atom which has been found to be important for the properties of the complexes.[12,14]

Vibrational spectroscopy offers good possibilities to study trans effects in coordination chemistry, by means of the metal−ligand force constants and interaction terms. Oxygen coordination of pentacyano platinum complexes shows very slight

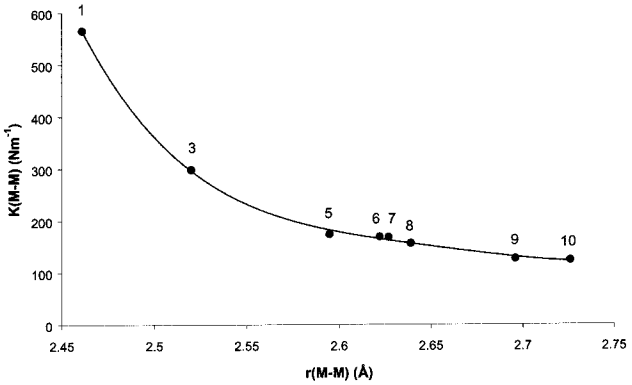

Figure 9. Correlation between metal−metal bond lengths and stretching force constants (cf. Table 11).

weakening of the axial trans Pt−C bond. The $K(PtC_{ax})$ force constants are only about 4−7% lower than $K(PtC_{eq})$, Table 9. In contrast, there is a much bigger difference between the equatorial and axial ligands in all dimetallic species. The PtC stretching force constants, trans to the metal−metal bond, are about 15−20% lower than the equatorial PtC values. The PtC stretching force constants indicate weak trans influence of the ligands X = H_2O, OH, Cl, Br, or I for the complexes $[Pt(CN)_5X]^{n-}$ (for halide compounds see Table 9 and ref 18). However, the metal−metal bonding for X = −TlCN, $-Tl(CN)_2$, $-Tl(CN)_3$, and $-Pt(CN)_5$ gives a strong trans influence. This again reflects the special nature of the metal−metal bond, especially for the $[(NC)_5Pt-Tl(CN)]^-$ complex in which the σ bonds along the C−Pt−Tl−C axis have been described as rather delocalized.[14] Despite this clear vibrational spectroscopic evidence of trans influence, no significant trend can be observed in the mean Pt−C bond distances obtained from the EXAFS studies.

2. PtO Stretchings. The Pt−O stretching frequencies for the $[Pt(CN)_5(H_2O)]^-$ and $[Pt(CN)_5(OH)]^{2-}$ complexes were assigned to very close frequencies about 545 cm^{-1}. Consequently, the Pt−O stretching force constants are close (Table 9) or even slightly higher for the H_2O complex, as 268 Nm^{-1}. We expected a stronger Pt−O bond with OH than with H_2O as ligand. If one assigns the band at 502 cm^{-1} in the spectrum of $[Pt(CN)_5(H_2O)]^-$ as the Pt−O stretching mode (Table 8), then the corresponding refined force constant would be 229 cm^{-1}. In this case, the Pt−OH_2 force constant is about 22% lower than the Pt−OH one. Using D_2O as a ligand would solve this assignment problem.

3. Metal−Metal Stretchings. The Pt−Pt bond is much weaker in the $[(CN)_5Pt-Pt(CN)_5]^{4-}$ complex, with a stretching force constant of 124 N m^{-1}, than the Pt−Tl bonds in the dimetallic $[(NC)_5Pt-Tl(CN)_n]^{n-}$ ($n = 1-3$) cyano species, with the force constants 174, 169, and 156 N m^{-1}, respectively. The Pt−Pt stretching frequency, 145 cm^{-1}, is close to the value 139 cm^{-1} obtained for the compound $[Pt(C_8H_{12}(NO)_2H)_2Cl]_2$ with an unsupported $Pt^{III}-Pt^{III}$ bond of 2.6964(5) Å.[6] The compound $[Pt_2Cl_2(acac)_4]$, characterized by NMR, showed a $Pt^{III}-Pt^{III}$ Raman stretching frequency of 144 cm^{-1}.[5] Thus, the Pt−Pt bond distance and strength in the present $[Pt_2(CN)_{10}]^{4-}$ species corresponds well to comparable values for single $Pt^{III}-Pt^{III}$ bonds. Figure 9 shows a clear trend with decreasing force constant for the metal−metal bond with increasing bond distance.

4. Method of "Spectroscopic" Masses. The platinum−platinum stretching vibration, occurring at 145 cm^{-1} in $[Pt_2(CN)_{10}]^{4-}$, involves the following displacements of the internal coordinates: Pt−Pt−C_{eq} deformations, linear PtCN bendings perpendicular to the equatorial plane, and Pt−C_{ax} and CN(axial) stretchings. The Raman band at about 466 cm^{-1} is dominated by the Pt−C symmetric (A_{1g}) stretching frequency and varies little for the $Pt(CN)_5$ groups in different complexes. The axial and equatorial modes were previously found at 467 and 433 cm^{-1}, respectively, for the $[(Pt(CN)_5I]^{2-}$ complex,[18] whereas they could not be observed separately for the $[Pt(CN)_5(H_2O)]^-$ and $[Pt(CN)_5(OH)]^{2-}$ complexes. For the $[Pt_2(CN)_{10}]^{4-}$ complex, the band at ~400 cm^{-1} is assigned to the axial Pt−C stretching mode, downshifted by the *trans* effect of the Pt−Pt bond.

As a rule, metal−metal bond stretchings couple strongly with coordinates along the metal−metal bond direction, and the vibrational force constant of the metal−metal stretches depends on the shape, size, geometry, etc. of the ligands. Therefore, ignoring the ligands to perform simplified force constant calculations by using only the masses of the metal atoms in the so-called diatomic model, can be a poor approximation.[12,51]

For the four dimetallic $[(NC)_5PtTl(CN)_n]^{n-}$ ($n = 0$, 1, 2, and 3) complexes of different charges, rigorous calculations gave the stretching force constants 168, 174, 169, and 156 N m^{-1} (Table 11), whereas the approximate diatomic model resulted in 151, 158, 156, and 149 N m^{-1}, respectively. Generally, the diatomic approximation, when based merely on the atomic masses of the metals, strongly underestimates the metal−metal force constants.[51]

We present here an attempt to improve the accuracy while keeping the simplicity of the approximate calculations by introducing so-called "spectroscopic" (effective) masses of the metal atoms instead of their actual atomic mass. The "spectroscopic" mass is obtained from the result of a rigorous normal coordinate analysis (Table 12), i.e., the effective G-matrix element, and thus contains an inherent correction for the influence of the ligands on the metal−metal stretching fundamental. With effective metal masses, the M−M stretching force

TABLE 11: Structural and Spectroscopic Data for Pt−Pt and Pt−Tl Dimetallic Complexes

No.	complex	ν(M−M) (cm^{-1})	K(M−M) (N m^{-1})	r(M−M) (Å)	ref
1.	$[Pt_2(SO_4)_4(H_2O)_2]^{2-}$	297	564.8	2.461(1)	52
2.	$[Pt_2(SO_4)_4(OH)(H_2O)]^{3-}$	236	343.9		52
3.	$[Re_2OCl_5(O_2CCH_2CH_3)_2(PPh_3)_2]$	216	298	2.52	55
4.	$[Pt_2(SO_4)_4(CN)_2]^{4-}$	215	277.2		52
5.	$(NC)_5PtTl(s)$	160	167.9[a]	2.627	19
6.	$[(NC)_5PtTl(CN)]^-$	164	173.6[a]	2.595	12
7.	$[(NC)_5PtTl(CN)_2]^{2-}$	163	169.3[a]	2.622	12
8.	$[(NC)_5PtTl(CN)_3]^{3-}$	159	156.3[a]	2.639	12
9.	$[Pt_2(C_8H_{12}(NO)_2H)_4Cl_2]$	139	126.7	2.696	6
10.	$[Pt_2(CN)_{10}]^{4-}$	145	123.8[a]	2.726	*b*

[a] From rigorous normal coordinate calculations. [b] This work.

TABLE 12: Estimated "Spectroscopic" Masses (M_S) of Heavy Metals (Atomic Mass ~200) in a Metal−Metal Bond as a Function of the Charge of the Complex

charge	"spectroscopic" mass	effective G matrix element G_{MM}[a]	reference complexes
−4	199	0.010055	$[Pt_2(CN)_{10}]^{4-}$
−3	210	0.009541	$[(NC)_5PtTl(CN)_3]^{3-}$
−2	217	0.009200	$[(NC)_5PtTl(CN)_2]^{2-}$
−1	220	0.009094	$[(NC)_5PtTl(CN)]^-$
0	223	0.0089807	$(NC)_5PtTl(s)$
+1	225[b]	0.008900[a]	
+2	226[b]	0.008800[a]	

[a] From rigorous normal coordinate analyses. The relation is $M_S = 2/G_{MM}$. [b] Estimated values.

constant can be calculated by the expression used for diatomic molecules, namely, $K(MM) = 4\pi^2c^2\nu^2(1/M_1+1/M_2)$ where M_1 and M_2 are the effective masses of the metal atoms. The spectroscopic masses of heavy metals (e.g., Pt and Tl) turn out to be slightly higher than their atomic mass and increase slightly with decreasing negative charge of the complex (Table 12). On the basis of these estimated spectroscopic masses of the metal atoms, we calculated Pt−Pt force constants for the $[Pt_2(SO_4)_4(H_2O)_2]^{2-}$, $[Pt_2(SO_4)_4(OH)(H_2O)]^{3-}$, $[Pt_2(SO_4)_4(CN)_2]^{4-}$, and $[Pt(C_8H_{12}(NO)_2H)_2Cl]_2$ complexes with different charges (Table 11). In addition, the Re−Re force constant for the $[Re_2OCl_5(O_2CCH_2CH_3)_2(PPh_3)_2]$ complex was evaluated to 298 N m^{-1}.

The correlation found between metal−metal force constants (summarized in Table 11) and metal−metal bond lengths nicely illustrates the usefulness of the approximate calculations using the spectroscopic masses for the metal atoms. The values obtained for the force constants in the diatomic approximation agree reasonably well with the results based on rigorous calculations (cf. Figure 9). However, as with all kinds of approximate calculations, the use of "spectroscopic" masses has several restrictions.

(1) The "spectroscopic" masses in Table 12 can be used only for heavy metals with the atomic mass close to 200.

(2) The approximation should give best results in the range of bond distances between 2.58 and 2.73 Å where we have a number of reference molecules treated rigorously with full normal coordinate calculations. For shorter bond distances, we need more experimental data, both spectroscopic and structural.

We believe that the force constants obtained by using "spectroscopic" masses come close to the results of rigorous solutions. The method can be used as a fast and simple way to judge about the metal−metal bond strength, and the force constant can be used as starting values for refinement procedures of a full solution.

Conclusions

The structure of the dimeric $[Pt_2(CN)_{10}]^{4-}$ complex with an unsupported Pt−Pt bond, 2.73(1) Å, has been characterized in dilute (0.035 M) solution by EXAFS methods. Also for the $[(Pt(CN)_5I]^{2-}$ complex, with iodide as a heavy backscatterer, a Pt−I bond distance of 2.66(1) Å could be obtained, despite the strong multiple scattering from the linearly coordinated cyano ligands. The similarity of the solution and solid-state structures of the $[Pt(CN)_5I]^{2-}$ and $[Pt(CN)_5(OH)]^{2-}$ complexes, shown by EXAFS and vibrational spectroscopy, has provided the basis for normal coordinate analyses of the vibrational spectra to obtain force constants for discussions of the bonding.

For transition metal cyano complexes, the 18-electron rule is found to be useful for rationalizing metal−metal bonded structures and a useful guideline in searching for isoelectronic complexes analogous to observed species. The general coordination principles are those expected from schematic MO diagrams for π-acceptor ligands, which show that all nine valence orbitals of the metal atom can participate in weakly bonding MOs. Lower coordination numbers with a formal electron count less than 18 are not uncommon, because of strongly covalent metal−ligand bonds in some cases and steric ligand−ligand repulsion in others. However, the 18-electron rule gives a definite limit for the maximum possible coordination number that can be expected for cyano complexes.

Despite the limited number of experimentally observed vibrational frequencies from Raman spectra of aqueous solutions, normal coordinate analyses could be performed after careful assignments on a number of complexes $[Pt(CN)_5X]^{n-}$ with the ligands X = H_2O, OH, Cl, Br, or I, which showed a weak trans influence. For metal−metal bonding, as for X = −TlCN, $-Tl(CN)_2$, $-Tl(CN)_3$, or $-Pt(CN)_5$, the trans influence is strong. Correlations between force constants and bond lengths have been made. By introducing a charge-dependent effective "spectroscopic" mass for heavy metal atoms in dimetallic complexes, metal−metal stretching force constants in good agreement with rigorously obtained values can be obtained in a simple way by means of the diatomic approximation.

Acknowledgment. The financial support of the Swedish Natural Science Research Council (NFR) is gratefully acknowledged. The authors thank the European Commission INTAS Program, Russian Foundation for Fundamental Research (RFFI 98-03-32651), Carl Trygger Foundation for Scientific Research, and Wenner-Gren Center Foundation for financial support and the Hungarian National Scientific Research Foundation (OTKA T025278). We gratefully acknowledge the Stanford Synchrotron Radiation Laboratory (SSRL) for allocation of beam time and laboratory facilities. SSRL is operated by the Department of Energy, Office of Basic Energy Sciences. The SSRL Biotechnology Program is supported by the National Institutes of Health, National Center for Research Resources, Biomedical Technology Program, and by the Department of Energy, Office of Biological and Environmental Research.

References and Notes

(1) Cotton, F. A.; Walton, R. A. *Multiple Bonds Between Metal Atoms*, Clarendon Press: Oxford, 1993; Chapter 8.4, pp 508−532.

(2) Miller, J. S.; Epstein, A. J. *Prog. Inorg. Chem.* **1976**, *20*, 1.

(3) Reis, A. H., Jr.; Peterson, S. W.: Washecheck, D. M.; Miller, J. S. *Inorg. Chem.* **1976**, *15*, 2455.

(4) Whangbo, M.-H.; Hoffman, R. *J. Am. Chem. Soc.* **1978**, *100*, 6093.

(5) Prenzler, P. D.; Heath, G. A.; Lee, S. B.; Raptis, R. G. *Chem. Commun.* **1996**, 2271.

(6) Baxter, L. A. M.; Heath, G. A.; Raptis, R. G.; Willis, A. C. *J. Am. Chem. Soc.* **1992**, *114*, 6944.

(7) Cini, R.; Fanizzi, F. P.; Intini, F. P.; Natile, G. *J. Am. Chem. Soc.* **1991**, *113*, 7805.

(8) Paul, R. L. Ph.D. Thesis, Australian National University, 1996.

(9) Berg, K. E.; Glaser, J.; Read, M. C.; Tóth, I. *J. Am. Chem. Soc.* **1995**, *117*, 7550.

(10) Maliarik, M.; Berg, K.; Glaser, J.; Sandström, M.; Tóth, I. *Inorg. Chem.* **1998**, *37*, 2910.

(11) Maliarik, M.; Glaser, J.; Tóth, I.; W. da Silva, M.; Zekany, L. *Eur. J. Inorg. Chem.* **1998**, 565.

(12) Jalilehvand, F.; Maliarik, M.; Sandström, M.; Mink, J.; Persson, I.; Persson, P.; Tóth, I.; Glaser, J. *Inorg. Chem.* **2001**, *40*, 3889.

(13) Russo, M. R.; Kaltsoyannis, N. *Inorg. Chim. Acta* **2001**, *312*, 221.

(14) Autschbach, J.; Ziegler, T. *J. Am. Chem. Soc.* **2001**, *123*, 5320.

(15) Maliarik, M.; Glaser, J.; Tóth, I. *Inorg. Chem.* **1998**, *37*, 5452, and references therein.

(16) (a) Huheey, J. E.; Keiter, E. A.; Keiter, R. L. *Inorganic Chemistry*, 4th ed.; HarperCollins College Publishers: New York 1993; Chapter 15. (b) Porterfield, W. W. *Inorganic Chemistry, a Unified Approach*, 2nd ed.; Academic Press: San Diego, 1993; Chapters 11−13.

(17) Pei, J.; Weng, L.; Li, X. *J. Electroanal. Chem.* **2000**, *480*, 74.

(18) Memering, M. N.; Jones, L. H.; Bailar, J. C. *Inorg. Chem.* **1973**, *12*, 2793.

(19) Jalilehvand, F.; Eriksson, L.; Glaser, J.; Maliarik, M.; Mink, J.; Sandström, M.; Tóth, I.; Tóth, J. *Chem. Eur. J.* **2001**, *7*, 2167.

(20) Maliarik, M. Compounds with Non-Buttressed Metal−Metal Bond between Platinum and Thallium. Model Systems for Photoinduced Two-Electron Transfer, Ph.D. Thesis, Royal Institute of Technology, Stockholm Sweden, 2001, http://www.lib.kth.se/Sammanfattningar/maliarik010601.pdf.

(21) Mink, J.; Mink, L. M. *Computer program system for vibrational analyses of polyatomic molecules.* Available from J. Mink, L. M. Mink; Department of Analytical Chemistry, Veszprém University, P.O. Box 158, H-8201, Veszprém, Hungary.

(22) Sheldrick, G. M. *Computer Program for the Refinement of Crystal Structures*; SHELX97; Sheldrick, G. M., Ed.; University of Göttingen: Göttingen, Germany, 1997.

(23) Blixt, J.; Glaser, J.; Mink, J.; Persson, I.; Persson, P.; Sandström, M. *J. Am. Chem. Soc.* **1995**, *117*, 5089.

(24) Ressler, T. *J. Synchrotron Rad*. **1998**, *5*, 118; *J. Phys. IV France* **1997**, *7*, C2−269.

(25) (a) Zabinsky, S. I.; Rehr, J. J.; Ankudinov, A.; Albers, R. C.; Eller, M. J. *J. Phys. Rev. B* **1995**, *52*, 2995. (b) Rehr, J. J.; Ankudinov, A.; Zabinsky, S. I. *Catal. Today* **1998**, *39*, 263. (c) http://Feff.phys.washington.edu/feff.

(26) Lindqvist-Reis, P.; Muñoz-Páez, A., Díaz-Moreno, S.; Pattanaik, S.; Persson, I.; Sandström, M. *Inorg. Chem*. **1998**, *37*, 6675.

(27) Trueblood, K. N. In *Accurate Molecular Structures, Their Determination and Importance*; Domenciano, A., Hargittai, I., Eds.; IUCr; Oxford University Press: New York, 1992; Chapter 8.

(28) Golub, A. M.; Köhler, H.; Skopenko, V. V. *Chemistry of Pseudohalides*, Elsevier: Amsterdam, 1986; Chapter 3.

(29) Washecheck, D. M.; Peterson, S. W.; Reis, A. H.; Williams, J. M. *Inorg. Chem.* **1976**, *15*, 74.

(30) Weiss, J. *Z. Naturforsch.* **1974**, *29B*, 119.

(31) Kuroda, R.; Neidle, S.; Ismail, I. M.; Sadler, P. J. *Inorg. Chem*. **1983**, *22*, 3620.

(32) (a) Faggiani, R.; Howard-Lock, H. E.; Lock, C. J. L.; Lippert, B.; Rosenberg, B. *Can. J. Chem.* **1982**, *60*, 529.

(33) Jones, L. H.; Smith, J. M. *Inorg. Chem*. **1965**, *4*, 1677.

(34) Kubas, G. J.; Jones, L. H. *Inorg. Chem*. **1974**, *13*, 2816.

(35) Schultz, A. J.; Coffey, C. C.; Lee, G. C.; Williams, J. M. *Inorg. Chem*. **1977**, *16*, 2129.

(36) Williams, J. M.; Keefer, K. D.; Washecheck, D. M.; Enright, N. P. *Inorg. Chem.* **1976**, *15*, 2446.

(37) Hollis, L. S.; Roberts, M. M.; Lippard, S. J. *Inorg. Chem.* **1983**, *22*, 3637.

(38) Appleton, T. G.; Byriel, K. A.; Garrett, J. M.; Hall, J. R.; Kennard, C. H. L.; Mathieson, M. T.; Stranger, R. *Inorg. Chem.* **1995**, *34*, 5646.

(39) Simon, G. L.; Adamson, A. W.; Dahl, L. F. *J. Am. Chem. Soc.* **1972**, *94*, 7654.

(40) Brown, L. D.; Raymond, K. N.; Goldberg, S. Z. *J. Am. Chem. Soc.* **1972**, *94*, 7664.

(41) Dunbar, K. R.; Heintz, R. A. Chemistry of Transition Metal Cyanide Compounds: Modern Perspectives. *Prog. Inorg. Chem*. **1997**, *45*, 283.

(42) Carter, R. L. *Molecular Symmetry and Group Theory*; Wiley: New York, 1998; Chapter 7.

(43) Gerloch, M.; Constable, E. C. *Transition Metal Chemistry*; Wiley-VCH: New York, 1994; Chapters 6 and 7.

(44) Dasgupta, T. P.; Beckford, F. A.; Stedman, G. *J. Chem. Soc., Dalton Trans*. **1993**, 3605.

(45) Bandel, G.; Platte, C.; Trömel, M. *Acta Crystallogr. Ser. B* **1982**, *38*, 1544.

(46) Thiele, G.; Wittmann, K. *Z. Naturforsch.* **1983,** *38B*, 674.

(47) Clark, R. J. H.; Kurmoo, M.; Galas, A. M. R.; Hursthouse, M. B. *J. Chem. Soc., Dalton Trans*. **1982**, 2505.

(48) Tanaka, M.; Tsujikawa, I.; Toriumi, K.; Ito, T. *Acta Crystallogr., Ser. C* **1986**, *42*, 1105.

(49) Siebert, H.; Siebert, A. *Z. Naturforsch.* **1967**, *22B*, 674.

(50) Ferraro, J. R.; Basile, L. J.; Williams, J. M.; McOmber, J. I.; Shriver, D. F.; Greig, D. R. *J. Chem. Phys*. **1978**, *69*, 3871.

(51) Nakamoto, K. *Infrared and Raman Spectra of Inorganic and Coordination Compounds*, 5th ed.; Wiley-Interscience: New York, 1997; Part A, Chapter I-3; Part B, Chapters III-15 and III-24.

(52) Griffith, W. P.; Mockford, M. J.; Skapski, A. C. *Inorg. Chim. Acta* **1987**, *126*, 179.

(53) Bencze, É.; Mink, J.; Pápai, I.; Butler, I. S.; Lafleur, D.; Gilson, D. F. R. *J. Organomet. Chem*. **2000**, *616*, 1.

(54) Cotton, F. A.; Kraihanzel, C. S. *J. Am. Chem. Soc.* **1962**, *84*, 4432.

(55) San Filippo, J., Jr.; Sniadoch, M. J. *Inorg Chem.* **1973**, *12*, 2326−2333.